Title

THE SOLUTION ABSORPTION SPECTRUM OF Bk3+ AND THE CRYSTALLOGRAPHY OF BERKELIUM DIOXIDE, SESQUIOXIDE, TRICHLORIDE, OXYCHLORIDE, AND TRIFLUORIDE

Author

Peterson, Joseph Richard.

Publication Date

1967-10-01

UCRL-17875

eg. 1

University of California

Ernest O. Lawrence Radiation Laboratory

THE SOLUTION ABSORPTION SPECTRUM OF Bk^{3+}
AND THE CRYSTALLOGRAPHY OF BERKELIUM DIOXIDE,
SESQUIOXIDE, TRICHLORIDE, OXYCHLORIDE, AND TRIFLUORIDE

Joseph Richard Peterson
(Ph.D. Thesis)

October 1967

DISCLAIMER

UCRL-17875

UNIVERSITY OF CALIFORNIA

Lawrence Radiation Laboratory
and Department of Chemistry
Berkeley, California

AEC Contract No. W-7405-eng-48

THE SOLUTION ABSORPTION SPECTRUM OF Bk^{3+} AND THE CRYSTALLOGRAPHY OF BERKELIUM DIOXIDE, SESQUIOXIDE, TRICHLORIDE, OXYCHLORIDE, AND TRIFLUORIDE

Joseph Richard Peterson

(Ph.D. Thesis)

October 1967

THE SOLUTION ABSORPTION SPECTRUM OF Bk^{3+} AND THE CRYSTALLOGRAPHY OF BERKELIUM DIOXIDE, SESQUIOXIDE, TRICHLORIDE, OXYCHLORIDE, AND TRIFLUORIDE

Contents

THE SOLUTION ABSORPTION SPECTRUM OF Bk^{3+} AND THE CRYSTALLOGRAPHY OF BERKELIUM DIOXIDE, SESQUIOXIDE, TRICHLORIDE, OXYCHLORIDE, AND TRIFLUORIDE

Joseph Richard Peterson

Lawrence Radiation Laboratory
and Department of Chemistry
University of California
Berkeley, California

October 1967

ABSTRACT

The work reported here is the beginning of a systematic study of the physical and chemical properties of berkelium and its compounds. A total of ~30 μg Bk^{249} was made available for use in this study. The procedures used to purify the Bk^{249} solution are discussed in detail, as are the analytical techniques used to evaluate the purity of the Bk sample following each purification cycle. Repeated purifications were necessary to maintain the Bk samples in a state of high purity, since Bk^{249} decays to Cf^{249} at the rate of ~0.2% per day.

The experimental techniques used to study the Bk^{3+} solution absorption spectrum are discussed. One of these techniques, using a newly developed, light-pipe, microabsorption cell, marks a significant advancement in the further development of experimental techniques suitable for heavy-actinide-element research. The composite results of the observed spectra yielded 16 Bk^{3+} absorption peaks in the wavelength region 320 to 700 mμ. The two most intense peaks observed were at 418 and 474 mμ. The experimentally determined, electronic energy levels of Bk^{3+} are compared with theoretically derived values; however, no attempt to fit the observed data to the theoretical energy level scheme is made. Mention is made of an unsuccessful attempt to observe the Bk^{4+} solution absorption spectrum.

A discussion of the techniques to prepare a series of compounds on a single, submicrogram sample of material is given. These techniques were employed to prepare five compounds of berkelium. The conditions used to prepare these five Bk compounds are given, along with a discussion of the treatment of the data obtained from x-ray examination of the compound samples.

All samples of BkO_2 exhibited the fluorite-type, face-centered cubic structure with the "purest" sample yielding a lattice parameter $a_o = 5.334 \pm 0.001$ A. The dioxide stoichiometry was assumed, as was that of the Mn_2O_3-type cubic sesquioxide. The "purest" sample of Bk_2O_3 yielded a cubic lattice parameter $a_o = 10.889 \pm 0.003$ A. The effect of time on both of these lattice parameters is noted. These lattice parameter error limits represent the 95% confidence interval reflecting only the internal consistency of the data for these particular preparations.

The structure exhibited by $BkCl_3$ samples was the UCl_3-type hexagonal structure having lattice parameters $a_o = 7.382 \pm 0.002$ A and $c_o = 4.127 \pm 0.003$ A. Samples of BkOCl exhibited the PbFCl-type tetragonal structure having lattice parameters $a_o = 3.966 \pm 0.004$ A and $c_o = 6.710 \pm 0.009$ A. The lattice parameter error limits reported for $BkCl_3$ and BkOCl are the 95% confidence interval calculated using the standard statistical method for the average of three independent determinations.

BkF_3 samples exhibited two crystal structures, a low-temperature, YF_3-type orthorhombic structure and a high-temperature, LaF_3-type trigonal structure. "Best estimates" for the lattice parameters of these two BkF_3 modifications are: $a_o = 6.70 \pm 0.01$ A, $b_o = 7.09 \pm 0.01$ A, $c_o = 4.41 \pm 0.01$ A (orthorhombic) and $a_o = 6.97 \pm 0.01$ A, $c_o = 7.14 \pm 0.01$ A (trigonal). The lattice parameter error limits reported here are empirical, reflecting the uncertainties in the derivation of the lattice parameters.

Comparisons of the lattice parameters of these berkelium compounds with those of similar actinide compounds consistently showed evidence of the "actinide contraction". Calculations of the Bk^{3+} radius from the crystallographic data of Bk_2O_3, $BkCl_3$, and BkF_3 are tabulated. With reference to these calculations the limitations of the concept of ionic radius are discussed.

I. INTRODUCTION

Until recently the limited availability of berkelium (symbol Bk) has precluded the possibility of an extensive study of its physical and chemical properties. Previous berkelium work has been limited primarily to tracer studies dealing with its ion-exchange behavior,[1-4] its tetravalent oxidation state,[3-6] and its basic nuclear properties.[7-16]

To compare and correlate the properties of the heavy actinide elements with those of other heavy elements, bulk properties of these actinide elements need to be known. In 1959 Cunningham[17] reported his studies to determine the absorption spectrum of Bk^{3+} in the visible range and the magnetic susceptibility of the tripositive Bk ion sorbed on a single bead of cation-exchange resin. The first structure determination of a compound of Bk was carried out in 1962 by x-ray diffraction of 0.004 μg of BkO_2.[18] More recently the spectroscopic properties of Bk have been studied, including the spark spectrum[19] and the absorption spectrum of both the trivalent and tetravalent ions in solution.[20] The present availability of microgram quantities of Bk^{249} led to the beginning of a systematic study of the physical and chemical properties of berkelium and its compounds.

Two primary difficulties are encountered in work on the microgram and submicrogram scale: (1) purification of the solutions and (2) development of suitable experimental techniques. The solutions to these purification and experimental problems, as applied to the Bk work, are discussed in this thesis.

Experimental techniques were devised, developed, and proven to be satisfactory on this scale of operation before use in Bk experiments. The microabsorption cell employed in the solution spectroscopic studies of trivalent and tetravalent Bk was a significant advancement in the further development of experimental techniques for small quantities of heavy actinide elements.

The preparations, crystal structures, and lattice parameters of BkO_2, Bk_2O_3, $BkCl_3$, BkOCl, and BkF_3 are discussed. The lattice parameters derived from these compounds are compared with those of the isostructural lanthanide and actinide oxides, halides, and oxyhalides.

II. SOURCES OF BERKELIUM; ITS SEPARATION, PURIFICATION, AND PURITY EVALUATION

A. Sources of Berkelium

Berkelium was first synthesized in December 1949 by the bombardment of milligram quantities of Am^{241} with 35 MeV helium ions in the Berkeley 60-inch cyclotron. Thompson, Ghiorso, and Seaborg identified the new element through its characteristic ion-exchange behavior and its 4.8 hr electron-capture decay.[22] Today eight different isotopes are known, the lighter ones synthesized by cyclotron bombardment, the heavier ones by long-term neutron irradiation of the lighter actinides.[23] The mass numbers, modes of decay and half lives of these eight Bk isotopes are listed in Table II-1. The only isotope of Bk available even in microgram quantities is 249.

This work was begun with a total of 2.5 μg Bk^{249}, produced as part of the heavy isotope production program of the U. S. Atomic Energy Commission. Experimental possibilities were expanded upon the receipt of an additional 28 μg Bk^{249}, recovered from completed experiments by the heavy element chemistry group at the Livermore branch of the Lawrence Radiation Laboratory.

B. Separation and Purification

The berkelium solutions were purified by solvent extraction and ion exchange. Both methods have received much attention in developing suitable separation procedures needed for the purification of the actinides.[24,25]

1. HDEHP Extraction

Following the procedure of Peppard, Moline and Mason,[26] the Bk was taken up in a 10 M HNO_3-0.1 M $KBrO_3$ feed solution. The bromate served as the oxidizing agent to keep the Bk in the tetravalent state. The Bk was then extracted from this aqueous nitrate solution with 0.15 M hydrogen di-(2-ethylhexyl)orthophosphoric acid (HDEHP) in heptane, followed by stripping of the organic phase with a 1.5 M H_2O_2-8 M HNO_3 solution. A detailed flow diagram for the entire extraction process is shown in Fig. II-1.

The oxidation conditions were chosen such that the only tetravalent actinide would be berkelium. This HDEHP extraction is highly specific for tetravalent cations, thus rendering the Bk free from gross contamination by

Table II-1. Isotopes of berkelium.[16]

Mass number	Modes of decay	Half life
243	ϵ,α	4.5 h
244	ϵ,α	4.4 h
245	ϵ,α	4.98 d
246	ϵ	1.8 d
247	α	1.4×10^{3} y
248	β^-,ϵ	23 h
249	β^-,α,SF	314 d
250	β^-	193.3 m

Legend: α = alpha, β^- = beta, ϵ = electron capture
SF = spontaneous fission; h = hours, d = days, y = years,
m = minutes.

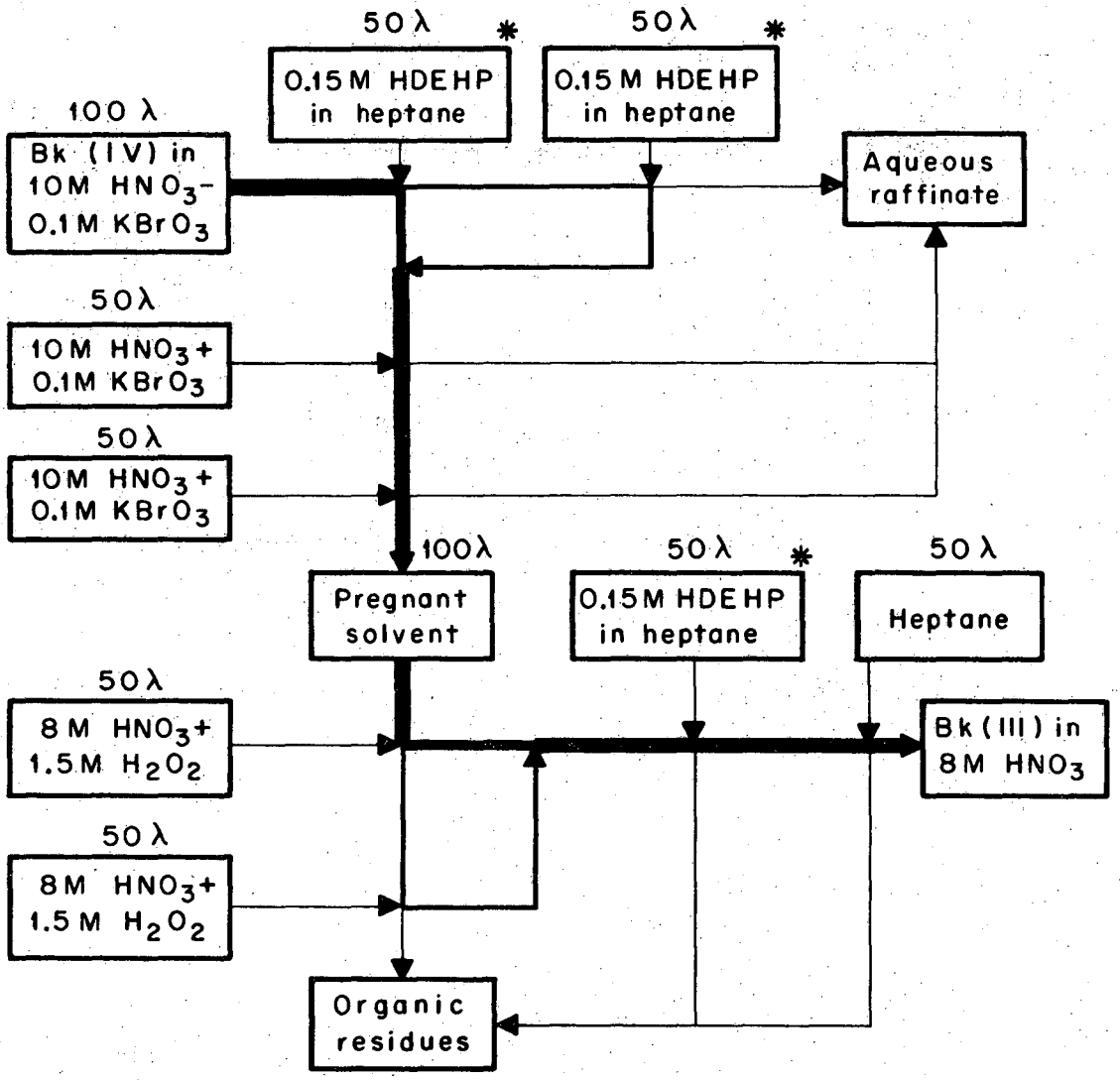

Fig. II-1. Flow diagram for Bk extraction using HDEHP (dark lines show Bk flow).

all the other actinides and lanthanides except cerium. Unfortunately, due to its similar oxidation behavior,[3] cerium is likewise extracted into the HDEHP phase, so at this point the Bk is potentially contaminated with gross amounts of cerium and lesser amounts of background contaminants, i.e., those coming from the reagents, containers, or air-borne laboratory dust.

Even after complete purification Bk^{249} is self-contaminating through its beta decay to Cf^{249} at the rate of ~0.2% per day, so repeated purification is necessary to maintain high purity. This HDEHP extraction is very effective for separating Bk and Cf.

As it was necessary to employ this extraction procedure several times during the course of this work, some additional experimentation with alternate extraction techniques was carried out. When employing the batch extraction method described above, it was very advantageous to use small volume phases, both with respect to mechanical handling ease and extraction efficiency. Small, rapidly tapered cones allowed good phase separations to be made. The smaller the solution volume, the higher the resulting Bk concentration and therefore the greater its purity with respect to background contaminants.

An alternate to batch extraction is chromatographic extraction.[27] Here a column bed of an inert matrix (e.g., diatomaceous earth or Kel-F) is used as a support medium for the HDEHP extractant. The extraction, scrub, and back-extraction are carried out by passing the various aqueous solutions through the column. In this manner the solutes of concern are allowed to partition many times between the aqueous and organic phases. Advantages of this technique are multiple extractions and ease of operation. However, it is markedly slower (about a factor of 2) and the back-extraction requires larger volumes of the H_2O_2-HNO_3 solution, thus diminishing the Bk concentration.

An alternative HDEHP chromatographic extraction procedure has been proposed by Kooi, Boden, and Wijkstra.[2] It avoids the use of oxidizing and reducing agents and requires only dilute HCl as eluant. Kooi's technique was not employed in this work, but it should be applicable to Bk-Cf separations, since the Bk elutes rapidly and ahead of the Cf.

2. <u>High-Purity Reagents and Containers</u>

Since the purity of the final Bk solution is limited by the purity of the reagents used in the final purification step, special precautions

were observed to ensure the highest possible purity of the HCl reagents. The high-purity HCl (H.P. HCl) reagents were prepared from water which had been doubly distilled from de-ionized water in a quartz still. Two milliliters of the quartz-distilled water (QD H_2O) to be used in the preparation of H.P. HCl reagents were evaporated down to ~50 µl in special Kel-F cones, then transferred to and dried down on copper electrodes for the analysis of cationic impurities by copper spark emission spectroscopy. The results of such an analysis, carried out by the emission spectroscopy group of this laboratory, are given in Table II-2. The QD H_2O samples were always "spectrochemically clean" (contaminants below the limits of detection) except for the possible presence of ~0.01 µg Ca (equivalent to ~5 ppb Ca).

The high-purity reagents were prepared and stored only in leached polyethylene bottles. No significant increase in impurities was found in these various H.P. HCl reagents when stored for a year in the leached polyethylene bottles. Room-temperature-saturated HCl was prepared in the apparatus drawn schematically in Fig. II-2. H.P. HCl solutions of the appropriate concentrations were prepared by suitable dilutions of the saturated HCl solution with QD H_2O. Saturated alcoholic-HCl solution was prepared at room temperature by saturating with HCl gas a 20 volume percent ethanol in concentrated HCl solution. Two milliliters of these various reagents were evaporated down and prepared for analysis of cationic impurities by copper spark emission spectroscopy. The analytical results for the three H.P. HCl solutions used in all of the final clean-up columns and for one sample of saturated alcoholic-HCl, freshly prepared for each column run, are listed in Table II-3.

A more detailed discussion of the reagent purification procedures can be found in Ref. 29.

Following the HDEHP extraction, the final purification steps were carried out under high-purity conditions. Only high-purity reagents were employed, and all containers used were leached quartz or polyethylene. Maximum Bk concentrations were maintained by minimizing solution volumes.

The leaching procedure for quartz used in high-purity operations is as follows:

(a) Wash with soap and water; rinse well with distilled H_2O.

(b) Soak in 1% HF-detergent solution for ~3 min; rinse well with distilled H_2O.

Table II-2. Spectrochemical analysis[a] of QD H_2O (plate no. 2202, μg/2 ml).

Al	< .01	Mg	< .01	Sn	< .1
Bi	< .05	Mn	< .01	Ta	< .1
Ca	< .01	Na	< 1	Ti	< .01
Cr	< .01	Nb	< .01	Y	< .01
Fe	< .01	Ni	< .05	Yb	< .01
K	< 1	Pb	< .1	Zn	< .1
La	< .01	Si	< .01	Zr	< .01

[a]The limits of spectrographic detection for common impurities are listed in Ref. 28.

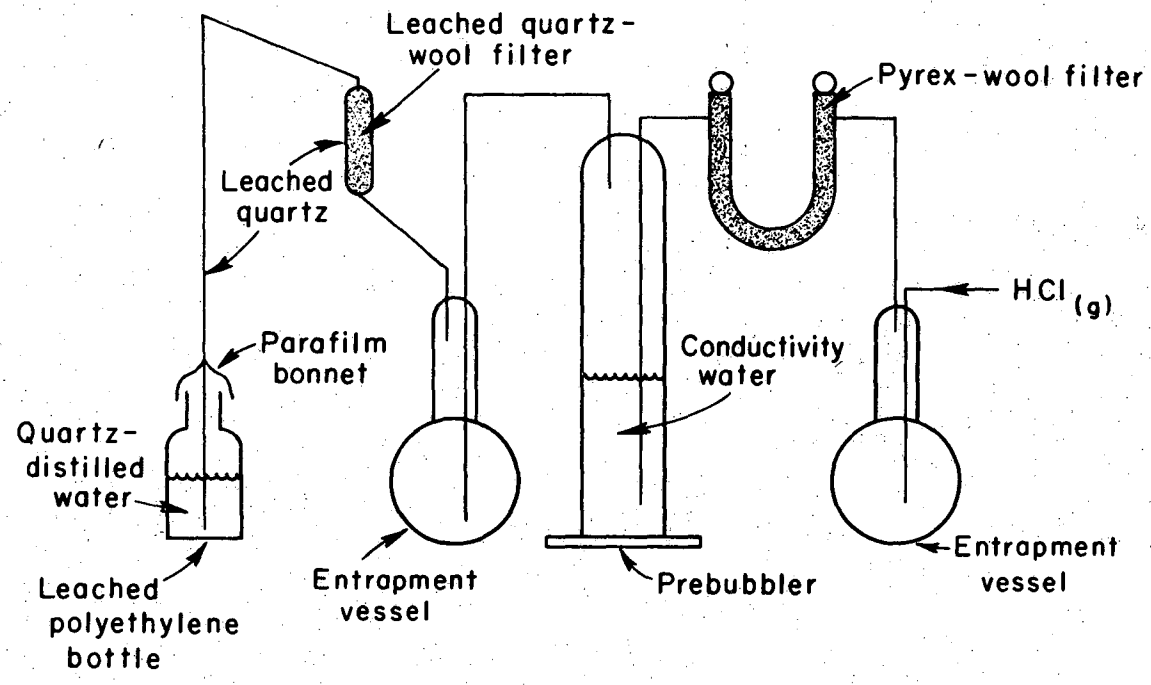

Fig. II-2. Apparatus for preparation of high-purity HCl solutions.

Table II-3. Spectrochemical analyses[a] of the high-purity reagents (μg/2 ml).

Impurities	6.3 M H.P. HCl, plate no. 2120	1.57 M H.P. HCl, plate no. 2121	0.05 M H.P. HCl, plate no. 2164	Saturated alcoholic-HCl, plate no. 2211
Ag	< .01	< .01	< .01	< .01
Al	< .01	< .01	< .01	.01
Be	< .01	< .01	< .01	< .01
Bi	< .05	< .05	< .05	< .05
Ca	~ .01	~ .01	< .01	.01
Ce	< .1	< .1	< .1	< .1
Co	< .05	< .05	< .05	< .05
Cr	< .01	< .01	< .01	< .01
Eu	< .01	< .01	< .01	< .01
Fe	< .01	< .01	< .01	< .01
K	< 1	< 1	< 1	< 1
La	< .01	< .01	< .01	< .01
Mg	< .01	< .01	< .01	< .01
Mn	< .01	< .01	< .01	< .01
Mo	< .01	< .01	< .01	< .01
Na	< 1	< 1	< 1	< 1
Nb	< .01	< .01	< .01	< .01
Ni	< .05	< .05	< .05	< .05
Pb	< .1	< .1	< .1	< .1
Si	< .01	< .01	< .01	< .01
Sm	< .05	< .05	< .05	< .05
Sn	< .1	< .1	< .1	< .1
Th	< .1	< .1	< .1	< .1
Ti	< .01	< .01	< .01	< .01
V	< .05	< .05	< .05	< .05
W	< .1	< .1	< .1	< .1
Y	< .01	< .01	< .01	< .01
Yb	< .01	< .01	< .01	< .01
Zn	< .5	< .5	< .5	< .5
Zr	< .01	< .01	< .01	< .01

[a]The limits of spectrographic detection for common impurities are listed in Ref. 28.

(c) Soak in hot 6 M HCl and allow to leach for several days.

(d) Rinse with and soak for several days in conductivity water (obtained from the first-stage overflow in the two-stage quartz still used for preparing QD H_2O).

(e) Repeat (d) above using QD H_2O.

(f) Remove excess QD H_2O from the quartz pieces and dry in an oven. Store covered.

The procedure for the treatment of the polyethylene bottles is essentially the same with the omission of step (b) and the oven-drying part of step (f).

3. Ion-Exchange Operations

The ion-exchange columns used were leached quartz, 1 mm in internal diameter, and loaded to a resin bed height of about 27 mm with -400 mesh Dowex AG 50W × 4 resin (< 10 ppm ash) which had been previously washed in 1 M, 6 M, 12 M, and alcoholic-HCl solutions. The resin was retained in the column by a small, leached, quartz-wool plug. The general rule for column pretreatment is to wash the resin bed with several column volumes of each type of solution that will be used during the column's purification operation. These columns were equipped with polyethylene tips selected to give drops of about 2 µl or less volume. These non-wetting tips minimize tip contamination by the radioactive solutions and provide the small drop size required for efficient fractionation. The small column diameter and tip make it necessary to operate these columns under pressure. It has become practice at this laboratory to use high-purity, dry nitrogen gas to pressurize the columns. The columns were sized such that the total load of actinide to be purified was less than 10% of the resin capacity. A photograph of a column in its final stage of operation is shown in Fig. II-3. The drop size is ~0.75 µl, and the free column volume (taken as ~1/2 the resin bed volume) is ~11 µl.

The column effluent was monitored by a solid state detector,[30,31] whose output was recorded on a strip chart recorder. Since the Bk^{249} betas are so weak, the method of detection was by counting alphas, both those from the alpha branching of Bk^{249} [11] and those from the Cf^{249} growing into the Bk^{249}. A photograph of the "berkeley box" and the radioactivity detection

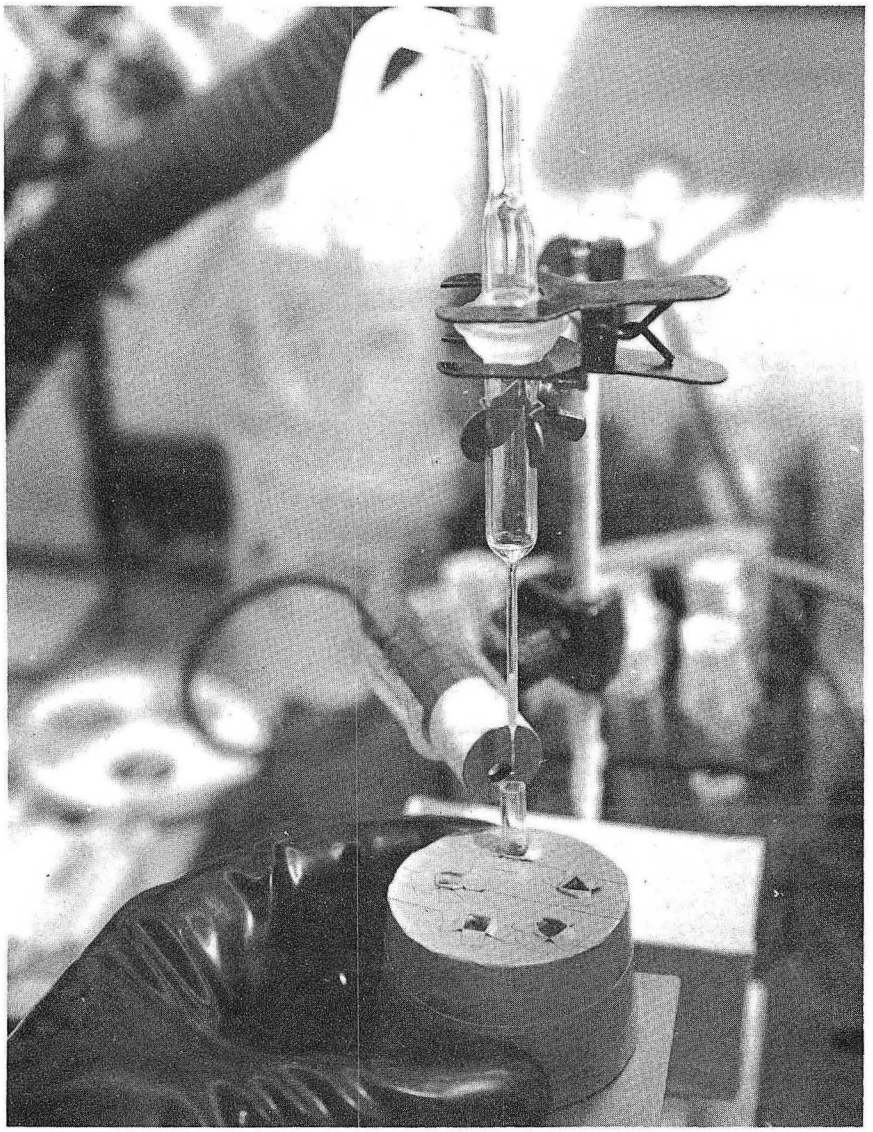

XBB 671-531

Fig. II-3. Ion-exchange column in final stage of operation.

and monitoring equipment is shown in Fig. II-4. The ion-exchange column can be seen in the center of the berkeley box.

Two columns were used in each purification cycle. The first, an alcoholic HCl, cation column,[32,33] effectively separates the actinides from the lanthanides. It was used in the Bk purification to separate out the gross amounts of cerium that could have come through the HDEHP extraction step. After pretreating the column as described above, it was operated as follows:

(a) The Bk was fed to the column in 0.05 M H.P. HCl. This low acidity sharply bands the activity at the top of the resin bed column, so large volumes of the acid could be used when necessary to transfer all the activity to the column and to rinse the upper column walls.

(b) Approximately two free-column volumes of 1.5 to 2 M H.P. HCl were passed through the column. This started the resin bed shrinkage and moved the activity band down the resin bed a short distance.

(c) The Bk was then eluted with HCl-saturated alcoholic-HCl solution.

(d) The activity was fractionated as indicated by the direct alpha count on the drops of effluent. The actinides and lanthanides elute in inverse order of their atomic numbers, so after the Bk activity was collected, the column was stopped.

The alcoholic HCl column was followed by a cation clean-up column[34,35] which, after pretreatment, was operated as follows:

(a) The activity was loaded as described for the alcoholic HCl column.

(b) 1.5 to 2 M H.P. HCl was placed on the column and elution was continued until the first sign of alpha activity in the effluent.

(c) The column was stopped; the remaining 1.5 to 2 M acid was removed and replaced with 6 M H.P. HCl for the elution of the activity. This served to strip the Bk from the column in as small a volume as possible.

After every column run, the activity distribution in the product fractions was determined by <u>in situ</u> counting of the Cf^{249} gammas (~390 keV).

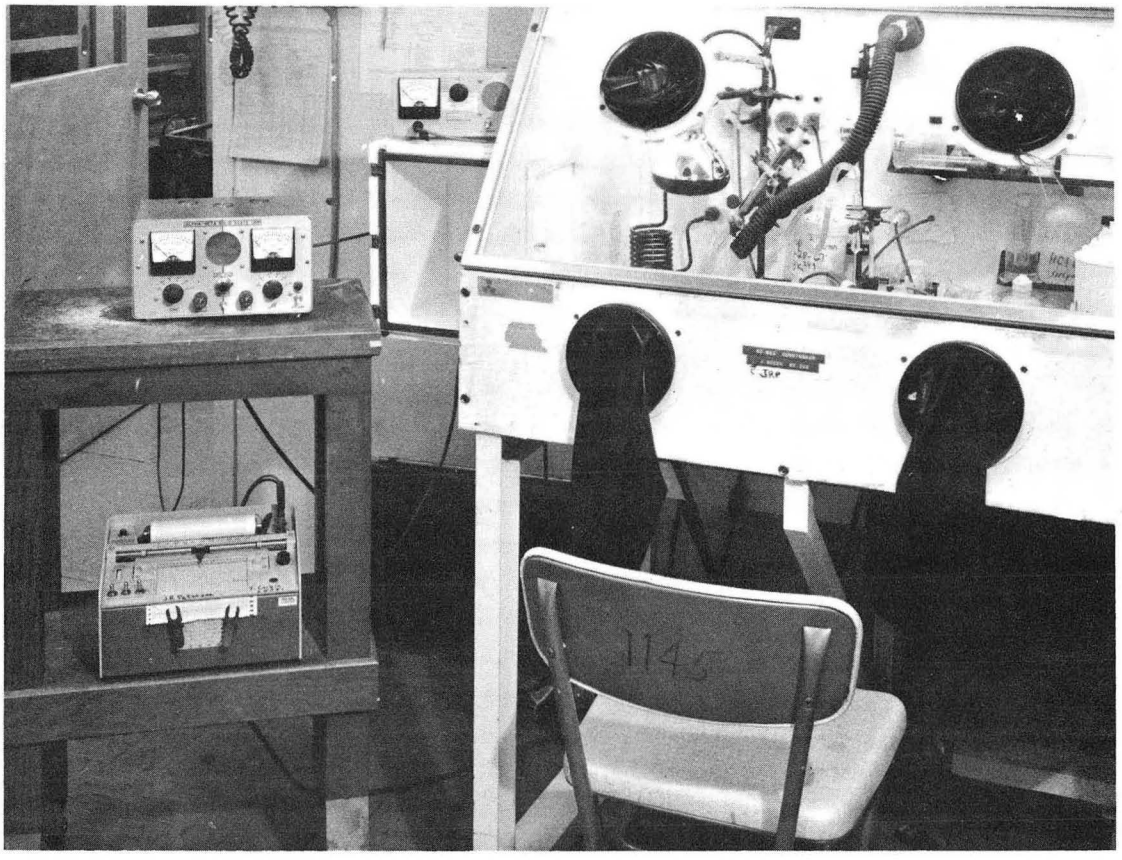

XBB 671-530

Fig. II-4. Berkeley box and radioactivity detection and monitoring equipment.

A NaI crystal and pulse height analyzer served as the detection and analysis system. Fixed "live-time" counting periods were used on each fraction, and from the resulting data, a percentage activity distribution was calculated. This eliminated the necessity for time-consuming, direct Bk assays during the ion-exchange operations.

4. Bk^{249} Assay Techniques

Accurate assays of berkelium solutions have long been a problem. The most widely-used method is based on the growth of Cf^{249} alpha activity. In the interest of maintaining high purity, it was necessary to devise a variety of assay techniques that didn't require the time-consuming Cf^{249} alpha-growth analysis. A brief description of all of these assay techniques follows:

(a) Direct alpha

A freshly HDEHP-extracted berkelium sample was alpha counted and its mass calculated using the Bk^{249} alpha specific activity of 2.95×10^{4} α counts/min/μg. This number was derived from the 314-day, Bk^{249} half life[9] and the alpha branching ratio determined by Chetham-Strode and Silva ($1.41 \pm 0.03 \times 10^{-5}$)[11] corrected to a Cf^{249} half life of 320 years.[36]

(b) Alpha ratio

Berkelium samples containing a small amount of Cf^{249} were assayed by determining the Bk^{249}-alpha/total-alpha ratio using standard alpha-pulse-height analysis techniques and then by counting total alphas in a 2π solid state, alpha counter. Multiplication of these numbers yielded the total number of Bk^{249} alpha counts per minute, from which the mass of the Bk^{249} sample was readily calculated.

(c) Mass ratio

Berkelium samples containing moderate or larger quantities of Cf^{249} were capable of being assayed directly only if the date of the Bk-Cf separation was known and all the Cf^{249} present in the sample had come from the Bk^{249} decay. Neglecting minor decay products one can write:

$$\text{Total alphas} = Cf^{249} \text{ alphas} + Bk^{249} \text{ alphas}$$

From the first-order decay law and the 314-day half life of Bk^{249}, one can calculate the percentage composition of a purified Bk^{249} sample at any future time. The ratio of these percentages gives the existing mass ratio of the sample, e.g., 80% Bk^{249} and 20% Cf^{249} (~100 days of Bk^{249} decay) corresponds to a Bk^{249}/Cf^{249} mass ratio of 4 to 1. If one lets x = mass of Cf^{249}, then 4x = mass of Bk^{249}, and one can write:

$$\text{Total alpha counts/min} = x(4.95 \times 10^{6}\ \alpha \text{ counts/min}/\mu g) + 4x(2.95 \times 10^{4}\ \alpha \text{ counts/min}/\mu g).$$

Therefore, by measuring the gross alpha count, one can calculate the mass of Bk^{249} in the sample, i.e., 4x.

(d) Cf^{249} alpha growth

Berkelium samples relatively free of Cf^{249}, or containing only small quantities thereof, can be assayed by the alpha-growth technique. This method requires periodic, gross-alpha counting. From the Cf^{249} alpha growth observed and the growth number of 11 alpha counts per minute increase per day per nanogram of Bk^{249}, one can calculate the mass of Bk^{249} in the sample.

C. Evaluation of Sample Purity

Several independent methods were applied to ascertain the purity of the final berkelium solutions. The analytical techniques used were mass analysis by isotopic dilution, alpha pulse height analysis, Cf^{249} growth from the beta decay of Bk^{249}, and emission spectrographic analysis using copper spark excitation. Knowledge as to sample purity with respect to gross contamination came from interpretation of the experimental results in the chemical studies, notably the solution absorption work and the observed lattice parameters of the various berkelium compounds.

1. Mass Analyses

After each complete purification cycle, samples containing ~20 ng of Bk^{249} were submitted for determination of total cerium and/or total neodymium content by mass analysis. The method employed was that of

isotopic dilution,[37] where an isotopically enriched "spike" solution is mixed with the unknown, whose contaminants being "spiked" are assumed to be in their natural isotopic abundance. This latter assumption was checked on the initial Bk samples, as they very well could have contained fission-product isotopic abundance rather than their natural isotopic abundance. This result also demonstrated that the chemical separations were working and that the main problem was to minimize the probability of background contamination from reagents, containers and air-borne laboratory dust.

To perform such mass analyses one requires a standardized, appropriately enriched "spike" solution, reagents of very high purity with respect to the element of interest, and a suitable, low-background filament system in the mass spectrometer. Despite its extreme sensitivity the high cost of time and effort to prepare and analyze these mass samples limited the analyses to Ce and Nd only. Cerium was chosen because of its Bk-like behavior in the HDEHP extraction part of the purification scheme; Nd, to indicate other rare earth contamination levels. A summary of results of the mass analyses is given in Table II-4. The 6.3 M H.P. HCl was analyzed for Ce since the berkelium was stripped off the final clean-up column in this reagent. This result demonstrated that the cerium content of the high-purity reagents was negligible.

2. Actinide Analyses

Although the purification chemistry specifically separated the Bk from all other actinides, actinide analyses were performed by standard alpha-pulse-height counting techniques. No alpha peaks other than those of Bk^{249} and Cf^{249} were observed in any of the analyses, with the exception of a small Cf^{252} alpha peak in the original 2.5 μg Bk^{249}. As no alpha peaks were observed, only upper limits of possible contaminating isotopes could be determined, by using the ratio of the maximum number of counts in the Bk^{249} alpha peak to the maximum number of counts in the energy range corresponding to the alpha peak of the suspected contaminating isotope. Often these peak channels were sufficiently close to the low-energy side of the Bk^{249} or Cf^{249} peak channels that they were significantly populated by degraded alphas from these major peaks. The results of recent determinations of the main alpha groups of Bk^{249} and Cf^{249} are given in Table II-5. Results of these actinide analyses are

Table II-4. Results of mass analyses.

Sample description	Sample size	Maximum[a] natural cerium (atom %[b])	Maximum[a] natural neodymium (atom %[b])	Berkelium isotopic composition
6.3 M H.P. HCl	1 ml	2.2×10^{-5} ng/μl	-	-
Bk^{249} from LRL-Livermore	10 ng	108	-	-
Bk^{249} purified 5/66	23 ng	0.38	-	$\geq$ 99.99% 249
Bk^{249} purified 8/66	17 ng	0.27	0.06	-
Bk^{249} purified 1/67	22 ng	9.53[c]	0.05	$\geq$ 99.99% 249

[a] No background correction made. Filament blanks showed 2-4 pg total natural Ce, 0.6-1.0 pg total natural Nd.

[b] With respect to Bk^{249}.

[c] Believed to be the result of the alcoholic HCl column failing to work.

Table II-5. Main alpha groups of Bk^{249} and Cf^{249}.[38]

Alpha source	α-particle energy (MeV)	Intensity
Bk^{249}	5.412±0.002	69.2±1.5
	5.384±0.002	18.4±0.5
Cf^{249}	5.808±0.003	82.6±0.3
	5.754±0.003	4.8±0.2

listed in Table II-6. The only source of actinides in the later berkelium samples was the decay of the berkelium itself.

3. Cf^{249} Growth

Using the Bk^{249} $T_{1/2}$ = 314 days and knowing the dates of the Bk-Cf separations, the amount of Cf^{249} grown into a given Bk sample at any time was readily calculated. This number was of particular importance in interpreting the observed lattice parameters of the various berkelium compounds prepared. A Bk sample will contain 5 atom % Cf^{249} in just 23 days after the Bk-Cf separation.

4. Emission Spectrographic Analyses

Emission spectrographic analysis of the purified Bk solutions was not feasible, because of the necessity of large quantities of Bk in order to obtain useful numbers. The applicability of this technique was limited to reagent analyses, where two milliliters of solution could be evaporated down and prepared for analysis. The results of some of these analyses are given in Tables II-2 and II-3 in Sec. II-B.

In summary, Bk solutions were purified by an HDEHP extraction followed by standard cation ion-exchange separations performed under high-purity conditions. Purity evaluation was made by both chemical arguments and direct analytical techniques, based primarily on mass analyses and emission spectrographic analyses. The Bk solutions were usually purified to the extent that the major contamination was from the decay of the Bk^{249} itself. This rapid decay necessitated repeated purification of the Bk^{249} solution. It was necessary, therefore, to carefully examine all experimental results obtained in view of the known contaminants, as determined for each Bk solution at the end of a purification cycle and determined for each Bk sample by the date of the last Bk-Cf separation.

Table II-6. Results of actinide analyses.

Bk sample description	Isotopes / Specific activity (α cpm/μg)[a]	Pu^{239} 7×10^4	Am^{241} 3.6×10^6	Am^{243} 2.1×10^5	Cm^{245} 1.8×10^5	Bk^{249} 2.95×10^4	Cf^{249} 4.95×10^6	Cf^{250} 1.6×10^8	Cf^{252} 6×10^8
assay plate after 11/65 Bk-Cf sep'n 11/10/65	maximum counts detected	< 15	< 10	< 55	< 500	906	332	< 115	481
	content (atom %)	< .73	< .009	< .87	< 9.19	-	0.22	< .002	0.003
LRL-Livermore material before pur'n 3/31/66	maximum counts detected	< 20	< 40	< 40	< 450	1280	3158	-	-
	content (atom %)	< .69	< .03	< .45	< 5.86	-	1.47	-	-
assay plate after 5/66 Bk-Cf sep'n 5/4/66	maximum counts detected	< 34	< 78	< 112	< 550	976	< 85	-	-
	content (atom %)	< 1.53	< .07	< 1.65	< 9.39	-	< .05	-	-
assay plate after 1/67 Bk-Cf sep'n 2/4/67	maximum counts detected	< 90	< 430	< 150	< 1800	3000	8632	-	-
	content (atom %)	< 1.32	< .11	< .72	< 9.99	-	1.71	-	-

[a] With the exception of Bk^{249} and Cf^{249}, all the specific activities were taken directly from Ref. 39. The Bk^{249} specific activity was based on a 314-day half life;[9] the Cf^{249} specific activity was based on a 320-year half life.[36]

III. SOLUTION ABSORPTION SPECTROSCOPY OF BERKELIUM

A. Introduction

The first attempt to observe the solution absorption spectrum of Bk^{3+} in the visible light region was carried out by Cunningham and colleagues in the late 1950's.[17] They attached a capillary absorption cell to the lower end of the ion-exchange column used in the final purification step, so that the purified material passed through the cell on its way to its final container. A bench spectrometer served as the light analyzer. From preliminary experiments using Am and Nd they concluded that they should be able to detect any Bk^{3+} absorption bands whose molar extinction coefficients (ϵ) were greater than or equal to 20. As they observed no absorption peaks over the wavelength range 4500 to 7500 A, this set an upper limit on the molar extinction coefficients of any Bk^{3+} absorption peaks in this wavelength region.

In 1963 Gutmacher and co-workers[40] published a preliminary report on the self-luminescence of the Bk^{3+} ion. A year later they reported[41] that the self-luminescence and absorption spectra of Bk^{3+} in a $LaCl_3$ crystal matrix had been obtained at 77°K. They found that the experimentally derived values of the low-lying energy levels agreed well with their calculated values for a $5f^8$ configuration. From attempts to observe the absorption spectrum of Bk^{3+} in solution, they concluded that the molar absorptivities of Bk^{3+} bands in the 2500-6800 A region must be less than 10. They were successful in observing 20 emission lines in the spark spectrum of berkelium using 0.1 μg quantities of Bk^{249}.[19,41] Some consideration was given to possible analytical utility of the Bk spark lines.

More recently cooperative experiments were performed at the Livermore branch of this laboratory to study in various acidic media the solution absorption spectrum of Bk^{3+} in the 3200-15,000 A region.[20] Sixteen absorption bands were observed. In addition, the Bk was oxidized to the tetravalent state and 6 lines of its absorption spectrum were seen. These results will be discussed in more detail later in this section.

During the course of this study two techniques were used to determine the solution absorption characteristics of berkelium. In general the two methods differed only in the way the Bk was contained or supported, for in both cases the measuring device was a Cary Model 14 Recording Spectrophotometer, equipped with a high-intensity light source (Cary Model 1471200).

B. Bk^{3+} on Single Cation Resin Beads

The idea of using a single, ion-exchange resin bead as a microabsorption cell for small quantities of actinides was explored by Cunningham and Thompson in 1958, when they attempted to observe the absorption spectrum of Bk^{3+} and Cf^{3+} absorbed in cation resin beads. They masked the bead from stray light by placing it in a close-fitting hole punched in a Pt disk, and they analyzed the transmitted light with a hand spectroscope. Later Cunningham and Wallmann demonstrated the potential of the single bead technique by observing the absorption spectrum of Am^{3+} using a similar experimental setup. They found that they could still see the 503 mμ Am^{3+} absorption peak (ϵ ~350) through the hand spectroscope with only 0.001 μg Am absorbed in the resin bead.[21]

In 1965 J. L. Green[29] made use of a single bead, microabsorption cell to observe the tripositive Cf ion absorption spectrum; then he extended the technique to a multibead stack to increase the effective path length and successfully intensified the observed spectrum.[42] Green also demonstrated, by comparing the known solution absorption spectrum of Pr^{3+} with observed Pr^{3+} bead spectra, that the observed bead spectra were very similar to the chloride solution spectra. Thus, the single bead technique provided a very convenient way to determine indirectly the solution absorption spectrum of tripositive Cf.

The cation-loaded resin beads are easy to manipulate, they constitute a 2 M concentration of actinide cation, and they have very good optical transparency in the visible and infrared regions. The main disadvantage is the lack of resolution in the bead spectra. In the case of Bk, another distinct disadvantage was that the bead didn't transmit light in the near ultraviolet region. Since Bk does much of its absorbing in this wavelength region, the technique was limited in its usefulness.

A schematic drawing of the single bead, microabsorption cell constructed for use in this study is shown in Fig. III-1. A high-purity, Dowex 50W × 4 resin bead, 181 μ in diameter, was loaded to saturation with ~1.6 μg Bk^{249} and placed in the cell. The loaded cell was attached to a brass disk which was positioned between a Zeiss ultrafluor uv objective and a Zeiss Achromat UV-Kond 0.8 condenser to optimize light transmission through the cell. The quartz objective served to focus the monochromatic Cary light beam onto the cell; the quartz condenser served to pick up the exit light beam from the cell for transmission to the Cary phototube. The quartz light-pipe above the bead made optical contact with the bead and served to catch much of the light scattered from the surface of the bead. Only a small percentage (< 1%) of the Cary light beam was transmitted through the cell system.

After the cell had been loaded with the Bk-containing resin bead, aligned in the light-condensing apparatus, and placed in the Cary Spectrophotometer cell compartment, the experimental procedure was to scan the visible and infrared wavelength regions, after maximizing the sensitivity of the Cary by adjusting the reference slit opening, the cell position in the Cary, the pen gain, and the Cary dynode setting. Multiple scans were made to confirm the reality of observed absorption peaks, usually seen as shoulders or small humps on the background, bead absorbance. The observation of a greater absorbance than that observed in the "empty bead" spectrum, as the wavelength decreased toward the uv, was interpreted initially as due to very strong Bk^{3+} absorption in this region.

In an effort to obtain greater resolution of the spectrum in this wavelength region, another 181 μ-diameter resin bead was partially loaded with ~0.6 μg Bk^{249}, by equilibrating it in a dilute HCl solution with the initial Bk-loaded bead. Wavelength scans to ~ 260 mμ on this bead showed a broad absorption peak between 285 and 310 mμ, which was attributed to Ce^{3+} contamination in the Bk. D. C. Stewart[43] reported an absorption peak (ϵ=18) at 296-7 mμ for Ce^{3+} in dilute $HClO_4$. The presence of cerium explained the rapid absorption noted in the initial Bk-bead spectra as the wavelength decreased toward the uv region. The presence of cerium added to the difficulty of picking out the Bk absorption peaks from the strong background absorbance; however, the Ce^{3+} did not introduce any

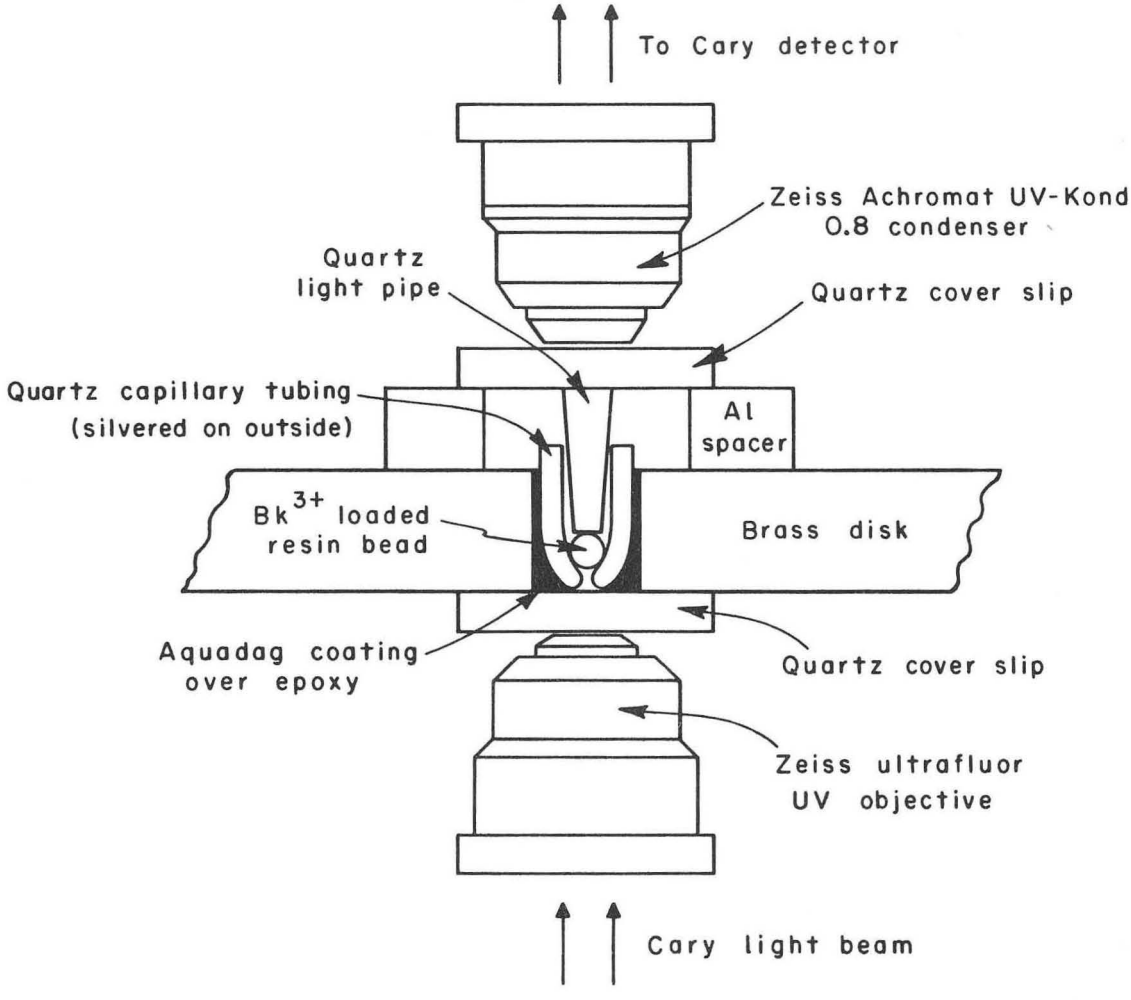

Fig. III-1. Single bead, microabsorption cell.

absorption peaks of its own in the visible region, since its absorption falls off rapidly as the wavelength increases from 300 mμ.

The results of the absorption spectral studies of Bk^{3+} absorbed in single, ion-exchange resin beads are listed in Table III-1. The Cary tracings were analyzed scan by scan. No attempts to resolve the Bk spectral features from the background absorbance were made. Peak positions were estimated by eye for each scan, and their reproducibility from scan to scan was considered good except for wavelengths below ~440 mμ. The lack of reproducibility in resolving the Bk^{3+} absorption peaks in this region prevents the listing of a definite set of absorption bands.

C. Bk^{3+} Solution on Light-Pipe Cell

Due to the lack of resolution in the Bk bead spectra, a new experimental technique was sought; one which had the capability of higher resolution and also allowed investigation into the ultraviolet wavelength region. The method chosen centered around the suspension of a drop of Bk solution between two, tapered, quartz rods. Prototype cells were constructed, loaded with drops of Nd solutions, and run on the Cary. Favorable results encouraged the development of such a "suspended drop" technique. The first "light-pipe" cell constructed for the Bk work, shown schematically in Fig. III-2, consisted of a 1 mm-diameter, quartz rod pulled down to slightly less than 100 μ in diameter and mounted in a brass disk, which served as an effective light mask. This "entrance light-pipe" was then aligned with and spaced ~200 μ from the "catcher light-pipe", a short section (~1 mm) of quartz rod slightly greater than 100 μ in diameter.

The Bk solution was transferred to the light-pipe gap as a small drop hanging on the end of a quartz micropipette, held firmly in a micro-manipulator. The hanging drop was formed by slow expulsion of the Bk solution from the micropipette and allowed to evaporate to a 0.5 μl volume for loading. After suspending the small drop of Bk solution containing ~1.5 μg Bk between the two rods, the cell was closed tightly, mounted on a large brass disk, and positioned between the quartz objective and condenser lenses as before. A H_2O-saturated atmosphere was maintained

Table III-1. Absorption spectra of Bk^{3+} absorbed in Dowex 50 resin beads.

Bk bead no. 1 ~1.6 μg (mμ)	Bk bead no. 2 ~0.6 μg (mμ)
638 ± 2	
500 ± 4	500 ± 4
475 ± 3	474 ± 2
458 ± 2	460 ± 2
432 ± 2	448 to 402[a]
423 to 392[a]	392 ± 2
378 ± 6	380 ± 4
	364 ± 4
	331 ± 3

[a]Lack of peak position reproducibility from scan to scan prevents listing of definite bands within this wavelength region, but evidence for Bk^{3+} absorption here was confirmed.

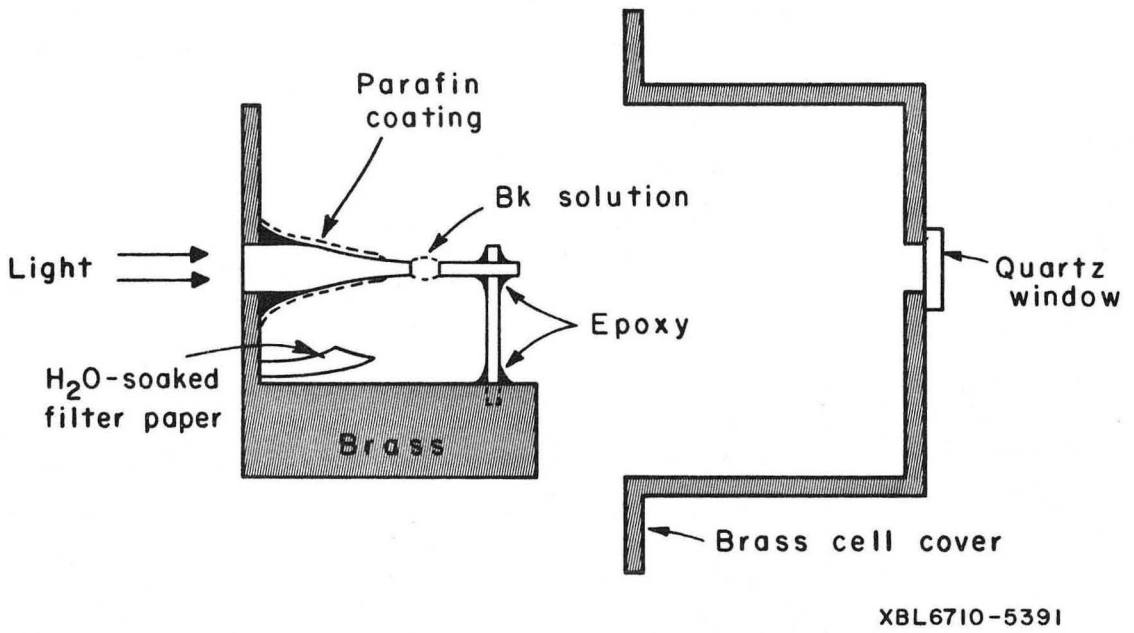

Fig. III-2. First light-pipe cell for Bk.

in the closed cell compartment by a H_2O-soaked piece of filter paper. The Cary infrared source lamp was a very effective heater to diminish the drop volume down to the few nanoliter size where the Bk concentration was maximized (3.8 M). With time the droplet increased in size by taking up H_2O from the cell atmosphere. Radiolytic decomposition of the aqueous Bk solution occurred at a negligible rate with respect to the wavelength scanning time.

A preliminary run with this cell, containing ~300 μg of Nd, yielded a spectrum over the wavelength range 2400 - 25,000 A showing all the known Nd^{3+} absorption peaks whose ϵ values are greater than or equal to 0.1. The Bk loaded onto this cell was that stripped off the two resin beads used in the previous absorption experiments and was used without any further purification. The observed spectra were very similar to the resin bead spectra previously discussed. New evidence for Bk^{3+} absorption lines was obtained in the 335-345 mμ wavelength region, at 420 ± 4 mμ and 440 ± 2 mμ. Again only a very small fraction of the Cary light beam was being transmitted through the cell system, and it became obvious that much improvement in this regard was necessary. Also realized was the necessity of having the Bk solution pure enough so that the droplet would remain a transparent solution at the high concentrations used. Salt formation in the drop drastically reduced the amount of light coming through the cell.

Improvement of the cell optics was the prime motivation for further developmental work on the light-pipe cell design, but other considerations were drop stability, control of the drop size, and mechanical handling ease. Over a period of time the cell optics were improved to the point where ~30% of the Cary light beam condensed by the ultrafluor objective was transmitted through the cell. These improvements were realized by shortening the length of the quartz, entrance light-pipe, by coating the entrance light-pipe with Ag or Al, by polishing the light-pipe ends, and by including a nearly spherical bulge in the entrance light-pipe to catch more of the incident light and to reverse the direction of back-reflected light.

Drop size was controlled by the heating effect of the Cary infrared source lamp and by the addition of dilute H.P. HCl solution. The addition of HCl solution was accomplished by a pump, a closed reservoir system operated by solution expansion induced by Pt-wire resistance heating. A photograph of the pump nozzle, positioned between the two, ~100 μ-diameter, light pipes, is shown in Fig. III-3.

The new cell design allowed greater ease in the loading, observation, and alignment procedures. This latter problem was solved by using a photoelectric cell to detect the maximum light transmission through the cell, while positioning the cell between the quartz objective and condenser lenses. A photograph of the open cell with its "slide-on" cover is shown in Fig. III-4. The overall length of the closed cell is ~2 in. Additional details of the light-pipe cell and its construction are given in Ref. 44.

When the second batch of Bk^{249} was received, absorption experiments were run with droplets containing ~4 μg Bk, loaded on the cell in about 0.06 μl volume. At minimum droplet volume this represented a 10 M Bk solution, however the usual operational volume kept the Bk concentration in the 3 to 5 M range. These concentrated Bk^{3+} solutions are emerald green in color.

A typical Bk^{3+} solution absorption spectrum observed on the Cary tracing over the wavelength range 320 - 680 mμ is shown in Fig. III-5. The high background absorbance in the lower wavelength region is probably caused by the presence of H_2O_2 and Cl_2, radiolytically generated from the aqueous HCl solution. In several experimental runs the presence of cerium added to this strong absorption as the wavelength decreased toward the uv region.

The list of the Bk^{3+} solution absorption peaks observed in this work, along with the observed wavelength variance for each peak, is given in Table III-2. The peak-position values are the statistical averages of eye-estimated peak positions from many wavelength scans over several independent experimental runs. No attempts to resolve the observed peaks were made. In addition to the absorption peaks listed, five questionable peaks below 315 mμ were observed. Although these peaks reproduced satisfactorily from scan to scan, their most probable peak positions were coin-

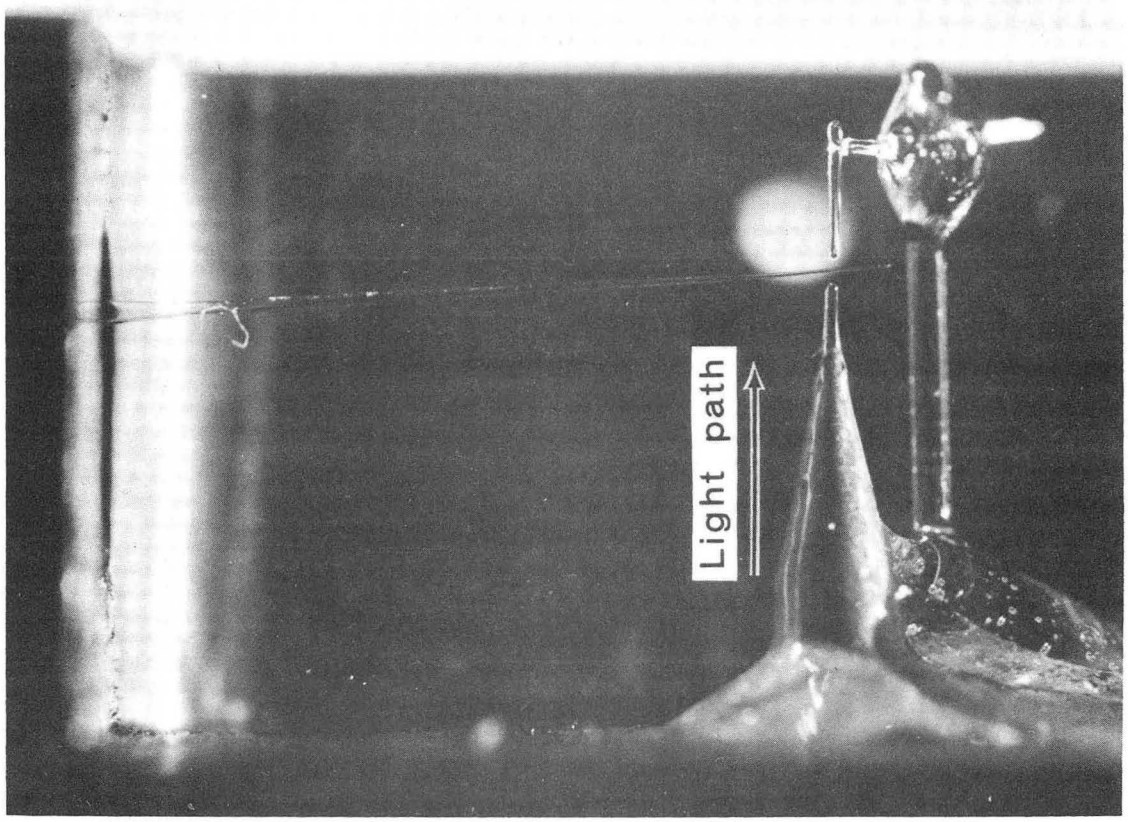

XBB 6710-6235

Fig. III-3. Light-pipe area of microabsorption cell showing pump-nozzle position.

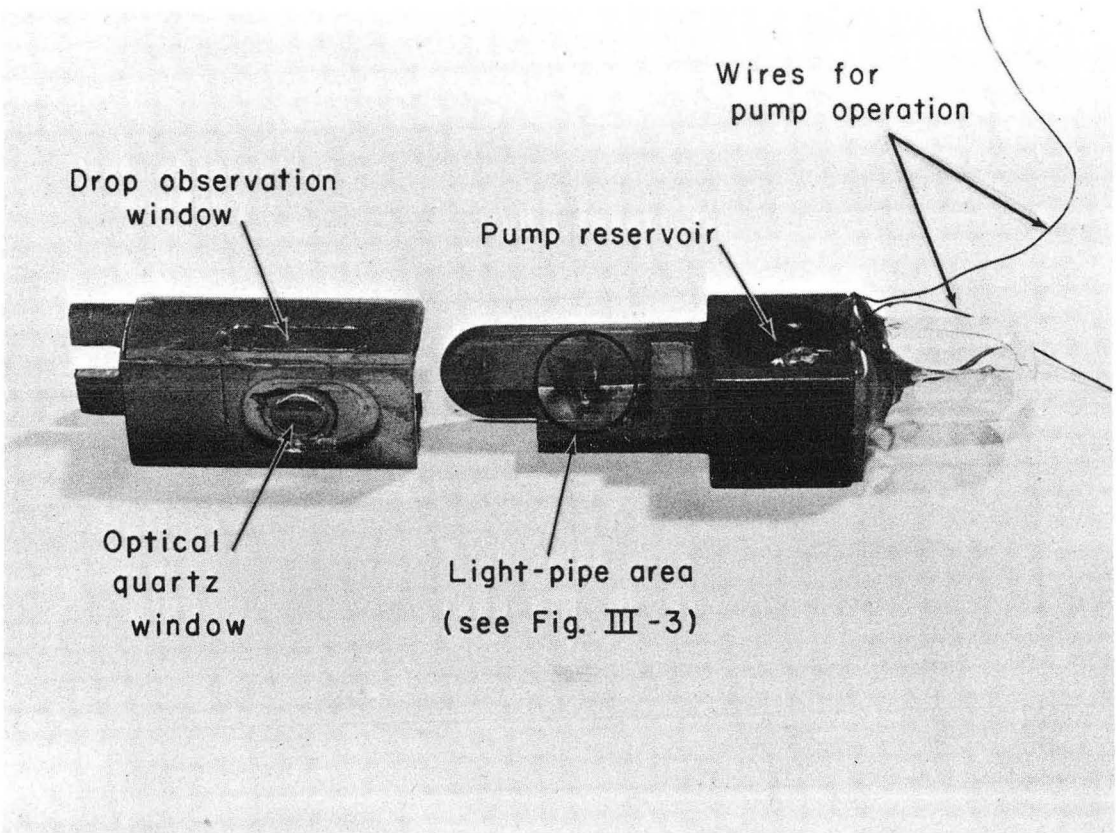

XBB 6710-6234

Fig. III-4. Light-pipe, microabsorption cell.

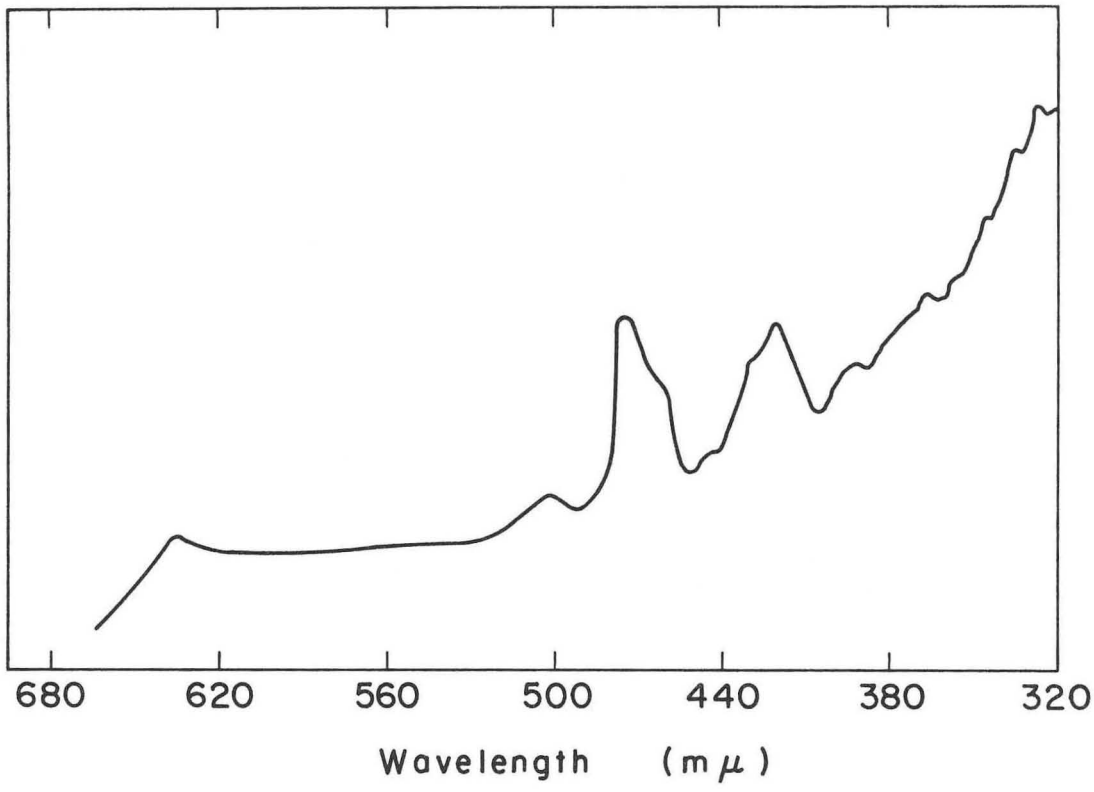

Fig. III-5. Bk^{3+} solution absorption spectrum.

Table III-2. Absorption spectrum of Bk^{3+} in dilute HCl solution.

Observed wavelength range (mμ)	Most probable peak position(mμ)	Peak description remarks
620 - 643	637	broad; moderate-strong; may be composed of several peaks
554 - 560	556	broad; weak
502 - 506	504	broad; moderate
484 - 487	485	small shoulder on strong peak
472 - 476	474	sharp; strong
459 - 464	462	moderate shoulder on strong peak
441 - 446	444	weak
428 - 433	430	moderate shoulder on strong peak
416 - 420	418	sharp; strong
395 - 398	396	weak shoulder on moderate peak
389 - 393	392	moderate peak on background absorption
376 - 380	378	small shoulder on background absorption
366 - 369	368	weak-moderate shoulder on background absorption
343 - 348	346	weak shoulder on background absorption
333 - 367	336	weak shoulder on background absorption
325 - 329	328	weak-moderate peak on background absorption

cident with similar peaks seen in the blank (empty cell) runs. More careful investigation in this wavelength region is necessary to establish the true identity of these peaks.

During the course of the Bk solution absorption work only a very few wavelength scans in the infrared region were made, because of a frequently inoperative Cary Spectrophotometer in this wavelength region. However, the scans that were obtained showed no evidence for any strong Bk absorption in the infrared region. The only peaks consistently seen, presumably due to H_2O absorption, were at ~1266 and ~1385 mμ. Contrary to these observations, the Livermore experimenters reported two strong Bk^{3+} absorption peaks in the infrared region, at 10,470 and 12,240 A.[20] This author is unable to explain why he didn't observe these peaks (if they are due to Bk), unless it is a function of the different solvents used (HCl verus DCl). In our experiments Cary tracings prominently showing the strong 474 mμ Bk absorption peak showed no evidence for strong Bk^{3+} absorption in the infrared region out to 20,000 A.

The Bk^{3+} solution absorption peaks observed in this work, those observed in the Livermore experiments in 1 M DCl solution, and the Livermore-calculated molar absorptivities are listed in Table III-3. The molar extinction coefficients of the various Bk^{3+} absorption peaks could not be calculated accurately in this work, since the exact concentration of the Bk solution was unknown and varied over any given wavelength scan. The agreement between observed peak positions is very good, with the exception of the two infrared peaks discussed above. Although the product of the Bk concentration times the path length of the absorption cell in the Livermore experiments was a factor of 3 to 5.5 smaller than that in our later experiments, they were able to improve significantly the statistical nature of their data by signal enhancement techniques. They accumulated data by a time-averaging device connected with their Cary Spectrophotometer through an automatic programming attachment. In theory this technique enhances the signal by a factor equal to the square root of the number of scans, while the random background noise is averaged out.

Table III-3. Observed Bk^{3+} solution absorption spectra.

This work, dilute HCl (mμ)	Livermore cooperative[a] experiments, 1 M DCl(A)	Livermore-calculated[a] molar absorptivities
not seen	12240	13
not seen	10470	6
637	6360	3
556	not seen	-
504	5040	1
485	not seen	-
474	4740	7
462	4600	3
444	4410	1
430	4300	2
418	4180	4
396	3958	0.5
392	3910	1
378	3744	0.5
368	3670	0.5
346	3450	1
336	3350	1
328	3275	1

[a]From Ref. 20.

D. Theoretical Interpretation of Absorption Spectral Results

Berkelium, the first element beyond the particularly stable $5f^7$ configuration of Cm^{3+}, is the only element in the second half of the actinide series known to have an oxidation state greater than 3. The general trends within the series indicate that berkelium absorption bands characteristic of both the trivalent and tetravalent oxidation states should occur within the visible range of the spectrum.[45] These predictions were confirmed by the observations of the Bk^{3+} solution absorption spectrum by this author and by Gutmacher et al.,[20] and by the observation of part of the Bk^{4+} solution absorption spectrum by Gutmacher et al.[20] These absorptions are attributed to f-f "forbidden" transitions with the berkelium.

This author has not attempted any theoretical fitting procedures or assignment of J-values to the various energy levels experimentally determined during the course of this work. Several years ago Carnall and Wybourne[46] demonstrated that there was a good correlation between calculated,"field-free" energy levels of the light,trivalent actinides and the solution absorption spectra of these ions. This indicates that, despite the greater spatial extension of the 5f orbitals over the 4f orbitals, the ligand field effects are of considerably less importance than the Coulomb and spin-orbit interaction energies. Their calculations were based on the assumption that the 5f radial wave functions are hydrogenic, so that values for the ratios of the Slater integrals F_4/F_2 and F_6/F_2 could be calculated, leaving only F_2 and the spin-orbit coupling constant, ζ, to be assigned values consistent with the experimental data. When it appeared that both of these parameters were linear functions of Z, Fields et al.[45] extrapolated linearly into the second half of the actinide series to get the parametric values necessary for making a complete intermediate coupling calculation for these elements. The validity of such a linear extrapolation is subject to question, but it did allow the start of theoretical calculations for the energy levels of the heavy actinides. Their calculations, using $F_2 = 299\ cm^{-1}$ and $\zeta_{5f} = 3260\ cm^{-1}$, indicated the energies at which absorption bands were expected, but they gave no information about the intensities for the various transitions.

Gutmacher[41] reported that he had performed similar calculations for the energy levels of the $5f^8$ configuration, using $F_2 = 285$ cm^{-1} and $\zeta_{5f} = 3135$ cm^{-1}, and that his experimentally derived values of the low-lying energy levels agreed well with his calculated values.

J. G. Conway[47] supplied this author with a copy of his "field-free" energy levels of Bk^{3+}, calculated in accordance with the procedure discussed by Wybourne[48] and outlined in Ref. 29. Conway used the following parametric values: $E^1 = 4600.0$ cm^{-1}, $E^2 = 16.2$ cm^{-1}, $E^3 = 410.0$ cm^{-1}, $\zeta_{5f} = 3200.0$ cm^{-1}, $\alpha = 39.0$ cm^{-1} and $\beta = -400.0$ cm^{-1} (γ was not used). The three E^n parameters are related to the Slater radial integrals, F_k, ζ is the spin-orbit coupling constant, and α and β are configuration interaction parameters.

A plot to compare the theoretically derived electronic energy levels of Bk^{3+} (as calculated by Fields et al.[45] in one case, and by Conway[47] in the other) with the experimentally observed Bk^{3+} absorption bands, as determined in this work, is shown in Fig. III-6. The numbers above the plotted lines in the two theoretical spectra are the J-values of the energy levels. The plot clearly shows that above ~18,000 cm^{-1} the density of levels is so great that no definite appraisal of the correspondence between the observed and calculated levels is possible.

Limited resolution in the solution absorption spectra makes the positive assignment of J-values to the various energy levels very difficult. The theoreticians can use the experimental data to refine their extrapolated parametric values, in as far as they are able to make their assignments agree with their calculations.

Qualitatively speaking, the intensities of the Bk^{3+} absorption bands are greater than those found for Tb^{3+}, the lanthanide homologue of berkelium, but smaller than those found for the absorption bands of the light actinides.

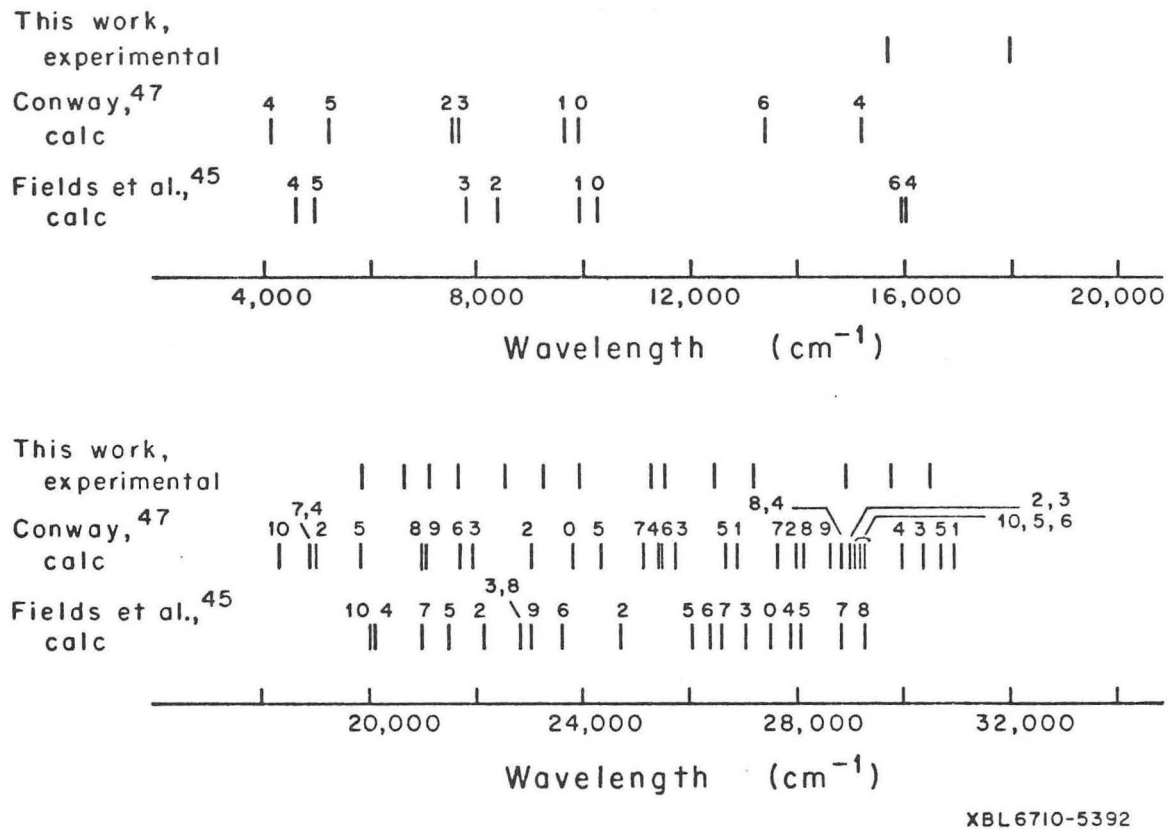

Fig. III-6. Observed and calculated electronic energy levels of Bk^{3+}.

E. Attempt to Observe the Bk^{4+} Solution Absorption Spectrum

An attempt to observe the tetrapositive berkelium solution absorption spectrum, by electrolytically oxidizing the Bk^{3+} in dilute HNO_3 solution while loaded on the light-pipe cell, was unsuccessful. While continuously scanning the visible region of the spectrum, several microamperes of current were passed through a microelectrode system inserted into the droplet in the light-pipe gap. The anode was a graphite fiber; the cathode, a copper wire separated from the droplet by a capillary salt-bridge. No real decrease in the Bk^{3+} absorption peaks or growth of peaks attributable to the 4+ state was observed.

Identical experiments carried out with comparable amounts of cerium (chosen because of its similar formal oxidation potential to berkelium)[3,6] worked very well. The failure with Bk was attributed to rapid reduction of the Bk^{4+} ions, formed locally at the anode, by radiolytically generated H_2O_2 in the bulk of the solution.

Gutmacher et al.[20] also had trouble oxidizing the berkelium to the tetravalent state, but finally succeeded in 5 M $HClO_4$, using $NaBiO_3$ as the oxidant. Their attempts using ozone in different solvent media were unsuccessful. Unfortunately, cerium was introduced as an impurity from the various reagents used in their oxidation attempts, so the Bk^{4+} absorption peaks were seen as shoulders on the stronger, Ce^{4+} absorption band. The Bk^{4+} absorption features that were repeatedly seen in three separate experiments with intervening purification procedures are listed in Table III-4.

Table III-4. Absorption peaks of Bk^{4+} in 5 M $HClO_4$ solution.[a]

Wavelength (A)	Estimated molar absorptivity
3610	b
3690	b
3950	8
4240	5
4380	3
5950	2

[a]Taken directly from Ref. 20.

[b]Not measurable.

IV. COMPOUND PREPARATION AND X-RAY DIFFRACTION STUDIES

A. Bead Loading and Ignition

The preparative technique employed in this work was that developed by Cunningham and Wallmann using single beads of cation-exchange resin.[18,21] Specially washed, sulphonic acid resin beads, ~90 μ in diameter, were loaded to saturation by equilibration with the purified Bk in a 0.05 M H.P. HCl solution. Once loaded, rinsed in QD H_2O, and air dried, these beads, each containing ~0.2 μg Bk^{249}, marked the starting point for the preparation of a series of compounds. The Bk-loaded resin beads were easily manipulated, represented a 2 M Bk concentration, and introduced only negligible chemical contamination to the Bk (ash content of the resin is less than 10 ppm).

The first step in preparing a compound from a Bk-saturated resin bead is illustrated in Fig. IV-1. The bead was placed on a thin, stationary, Pt wire and in turn this wire was placed inside a hole drilled in a Pt rod. A microtorch was used to heat slowly the Pt rod. During the ignition in air the bead underwent several distinct changes: from the initial, light yellow-orange color to black, as the carboneous bead-matrix material decomposed; then from black to light yellow as the sulphate formed; and finally to the yellow-brown (tan) color of the dioxide at a temperature greater than 1175°C. During this sequence the bead diameter decreased by a factor of 2, so at the completion of the air ignition the bead was a ~45 μ-diameter, coherent chunk of BkO_2. Using a quartz fiber attached to a micromanipulator as a dislodging tool, the sample was "chipped off" the Pt wire into a quartz capillary drawn out from a standard taper joint. At this point the capillary was either evacuated, sealed off, and aligned in the x-ray camera, or it was placed on the preparation vacuum line for *in situ* conversion of the dioxide to another berkelium compound.

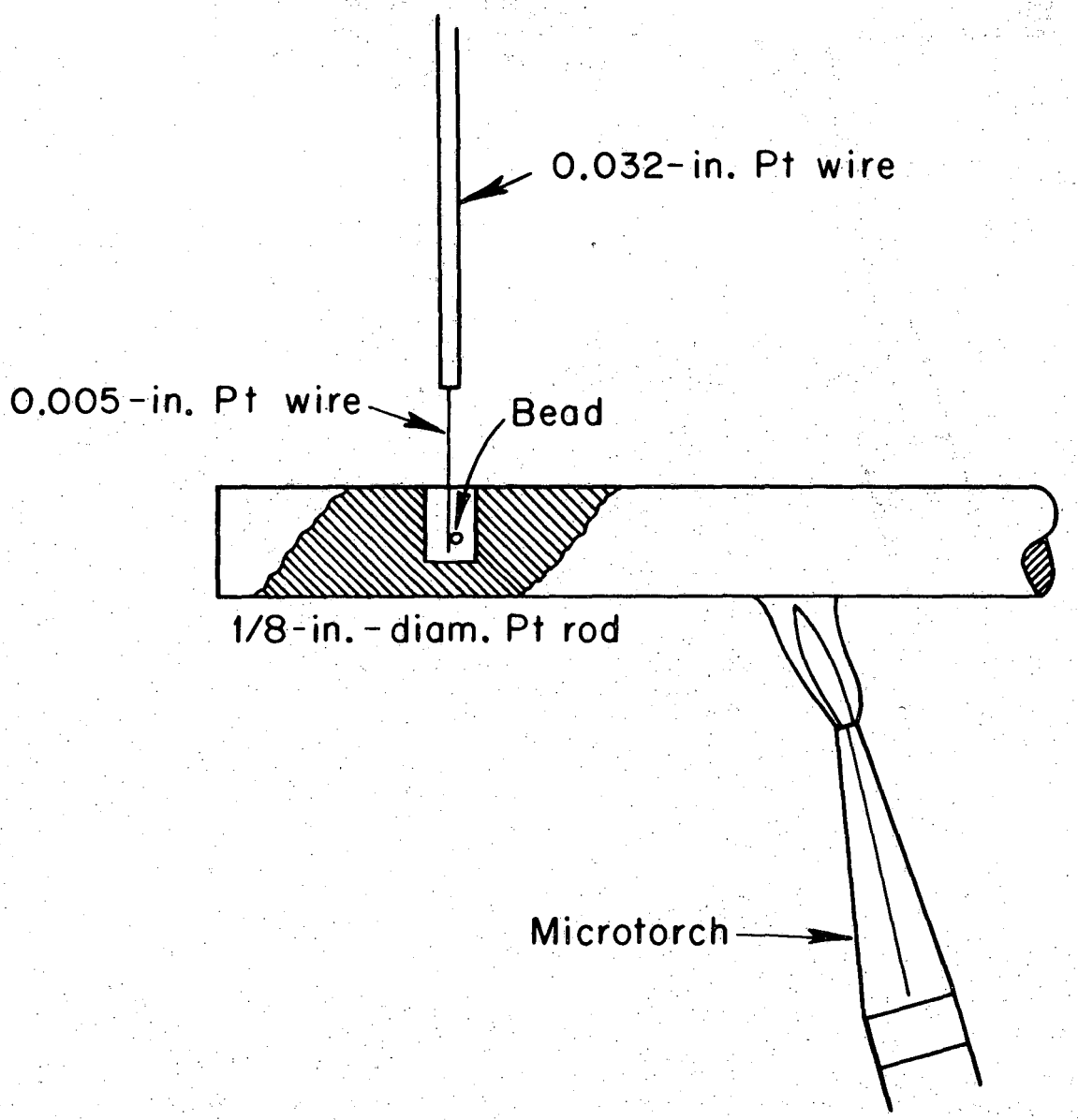

Fig. IV-1. Bead ignition apparatus.

B. Technique for Successive Compound Preparations

When the dioxide sample was to be submitted for x-ray analysis, the quartz capillary was evacuated and sealed off at a length of 30 to 40 mm in order that it could be cracked open again, following the x-ray work, and resealed onto its original standard taper using Apiezon W wax or quick-setting epoxy resin. Following this operation the berkelium sample was once again ready for in situ conversion to another compound. This process was repeated successively to prepare samples of berkelium sesquioxide, trichloride, and oxychloride. It was a very convenient and efficient technique to prepare a series of compounds on a single, 0.2 μg Bk sample.

C. Compound Preparation Procedures

The preparations of Bk_2O_3, low-temperature BkO_2, $BkCl_3$, and BkOCl were carried out on the preparation vacuum line shown schematically in Fig. IV-2. The sesquioxides were prepared by dry hydrogen reduction of the air-calcined (high-temperature) dioxides in accordance with the following procedure:

(a) The sample-containing capillary was evacuated, flushed several times with H_2 gas derived from heating UH_3, and evacuated to $\sim 10^{-6}$ mm Hg.

(b) The capillary was vented up to ~1/2 atmosphere H_2 (g) and the sample heated at 600°C for 20 min.

(c) The sample was quenched to room temperature, the capillary evacuated to $\sim 10^{-6}$ mm Hg and then refilled with another 1/2 atmosphere of fresh H_2 gas.

(d) Following another 20 min heating period at 600°C, step (c) above was repeated.

(e) After the third 20 min heating, the sample was quenched to room temperature and sealed off in ~1/2 atmosphere of H_2 gas for x-ray examination.

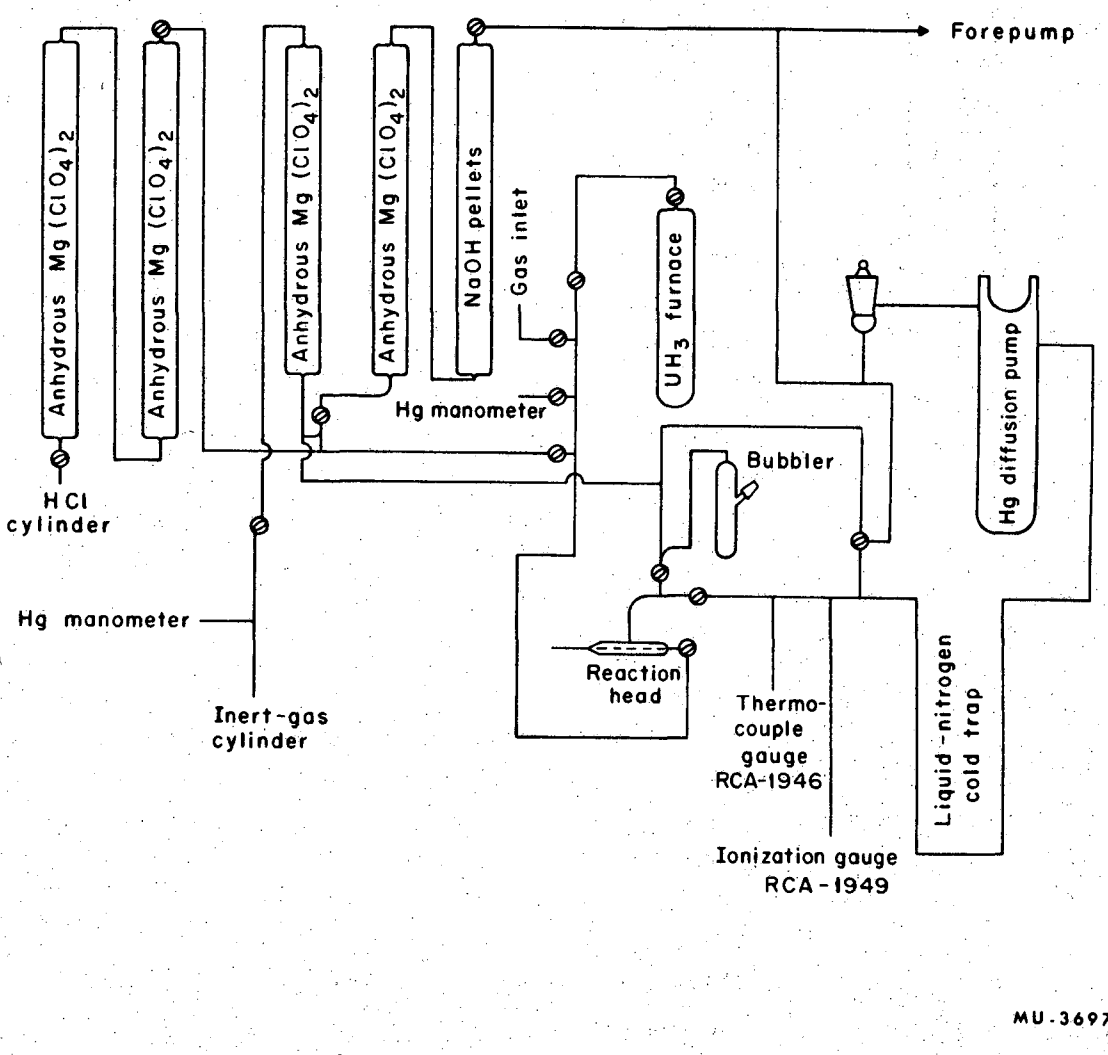

Fig. IV-2. Preparation vacuum line.

Conversion of the sesquioxides to the lime-green, anhydrous trichlorides was accomplished by treating in situ the oxide with anhydrous HCl gas at 520°C for three, 10-12 min periods interrupted by cooling, evacuation and admission of fresh HCl. Unlike the H_2 gas treatment, the HCl gas was passed through the system at atmospheric pressure.

The berkelium oxychlorides were also prepared utilizing a gas-flow system. Following initial evacuation and flushing, the anhydrous trichloride samples were treated at 500°C with an $HCl_{(g)}$-$H_2O_{(g)}$ mixture for three, 12-20 min periods. From the work of Koch[49] on the thermodynamics of the reation

$$AmCl_{3(s)} + H_2O_{(g)} = AmOCl_{(s)} + 2HCl_{(g)}$$

it was calculated that the vapor in equilibrium with a 9.5 to 10 M HCl solution should contain the proper HCl/H_2O ratio to drive the corresponding berkelium reaction to the right at 500°C. Matheson, high-purity, dry nitrogen gas was used as an inert carrier gas for the $HCl_{(g)}$-$H_2O_{(g)}$ mixture. The nitrogen was bubbled through the HCl solution at room temperature, passed through a quartz-wool plug to remove spray, then through the sample area at 500°C, and finally through an H_2SO_4 bubbler. Since the equilibrium constant favors trichloride formation at low temperature, the very pale green oxychloride samples were cooled in vacuum or in a dry nitrogen gas atmosphere.

Low-temperature berkelium dioxide was readily prepared by heating any of the above three berkelium compounds with air or oxygen at 600°C. The low-temperature BkO_2 samples appeared very similar to the sandy, or yellow-brown-colored, air-calcined dioxides.

To prepare berkelium trifluoride the initial bead ignition was carried out on a Pt wire attached to a portable Pt rod, drawn in Fig. IV-3. The entire Pt rod with dioxide sample was transferred to an all-Monel vacuum line, where it was treated in the following manner:

(a) The entire system was evacuated, flushed several times with tank H_2 gas, and filled with ~1 atmosphere of hydrogen gas.

(b) The tube furnace, surrounding the reaction area, was turned on, and the sample was heated to 600°C in the H_2 gas atmosphere.

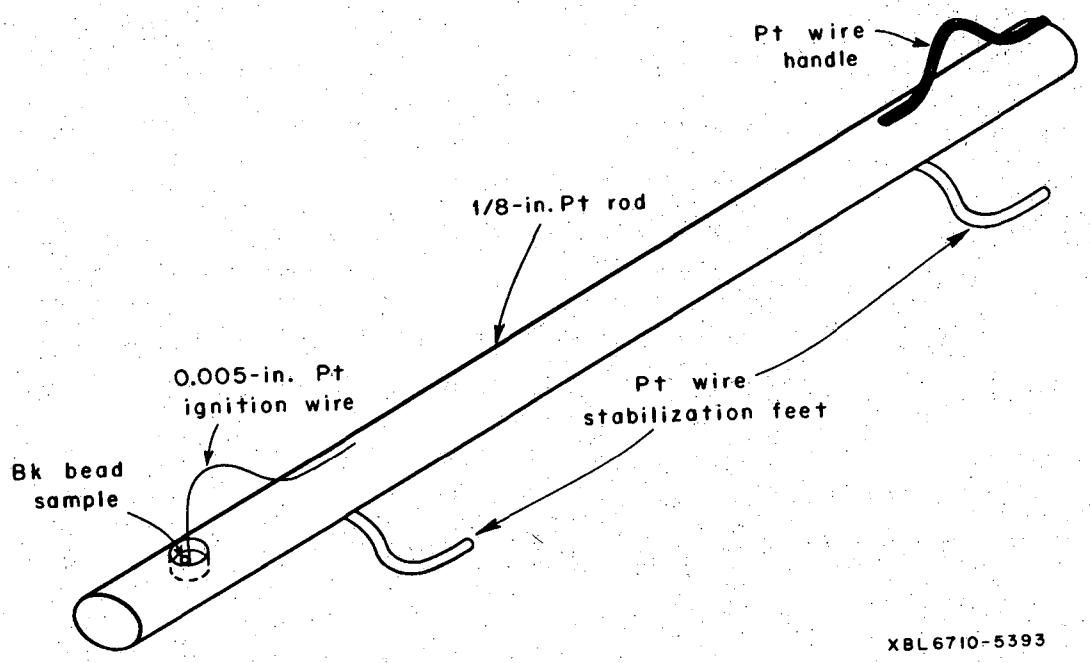

Fig. IV-3. Apparatus for hydrofluorination of berkelium oxide.

(c) At 600°C the hydrogen was pumped off and replaced with 300 mm of fresh H_2 gas and enough HF gas to bring the total pressure to 900 mm (to ensure no leaks into the system).

(d) After 30 min at 600°C the HF gas was condensed out with liquid N_2, the H_2 gas pumped off, and the system vented to a fresh $HF_{(g)}$-$H_{2(g)}$ mixture as before.

(e) Following a second 30 min heating period, the sample was either quenched to room temperature (by removal of the tube furnace) or allowed to cool slowly (by turning off the furnace and leaving it in place), depending on which crystallographic modification of the trifluoride was desired.

(f) When the sample was cool, the HF gas was condensed out, the H_2 gas evacuated, and the furnace flushed with Ar gas. The furnace was then filled to one atmosphere pressure of Ar gas for sample removal.

(g) The Pt rod was transferred back to the hood area where the BkF_3 sample was "chipped off" the Pt wire into a quartz capillary, which was subsequently evacuated and sealed off for x-ray examination.

The berkelium trifluorides were a very pale yellow-green color. The crystallographic properties of the bimorphic BkF_3 system are discussed in Sec. V-D.

Repeated attempts to prepare BkF_4 by fluorinating BkF_3 were unsuccessful. The failures were probably attributable to the reactivity of the tetrafluoride with the atmosphere. On this very small scale of operation a successful BkF_4 preparation will come from handling the fluorination product in an inert atmosphere. Successful preparations of CeF_4 on this 0.2 μg scale proved the applicability of the technique. For the fluorination reactions the sample container was constructed from a Monel rod, since the Pt rod reacted with the F_2 gas. After x-ray examination most of the amorphous, fluorinated samples were annealed <u>in situ</u> in their quartz capillaries to form berkelium trifluorides.

A flow diagram summarizing the conditions used in this study for the preparation of this series of berkelium compounds is presented in Fig. IV-4. Similar conversions could extend this series to include a

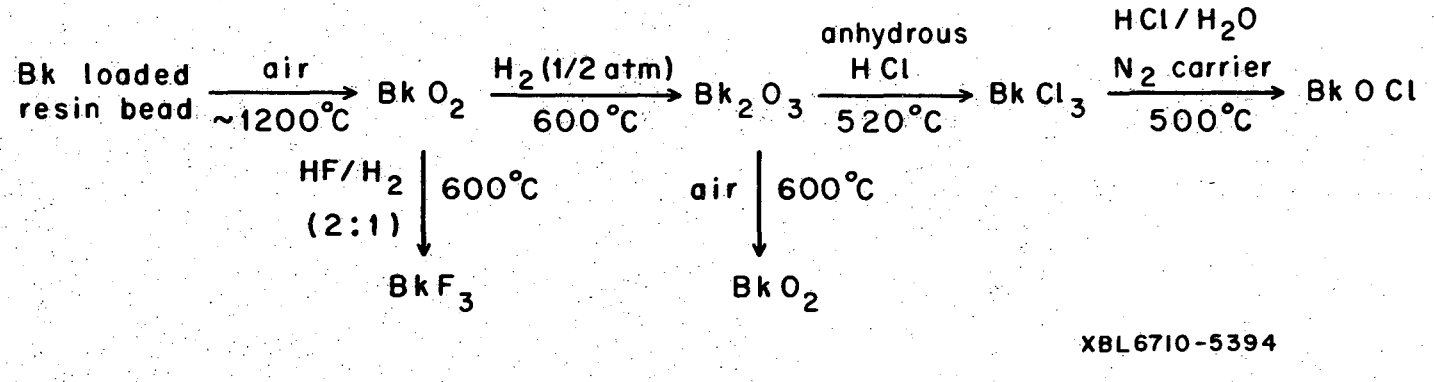

Fig. IV-4. Flow diagram for the preparation of a series of berkelium compounds.

great variety of additional berkelium compounds. Future work should certainly include other berkelium compound preparations, along with elemental Bk, to further elucidate the solid state chemistry of Bk and its compounds.

D. X-Ray Diffraction Equipment

All berkelium compound samples were examined by standard x-ray powder techniques. The diffraction equipment consisted of a Model 80-000 Jarrell-Ash Microfocus x-ray source and two, 57.3 mm-diameter, Debye-Scherrer type, Norelco Precision Powder Cameras[50] (suitably modified to accept the long capillaries), manufactured by the Philips Electronics Instrument Company. Exposure times varied from 8 to 16 hrs running at 45 kV- 3.5 mA and using Ilford G Industrial x-ray film. A 0.0003 in. Ni foil filter was placed inside the powder camera to remove the copper K_β x-rays and to help shield the film from the Bk^{249} radiations. The films were measured to a Bragg-angle precision of 0.05° on a Philips-Norelco film reader.

Both cameras employed in this work were calibrated by using a metallic gold standard to obtain sample x-ray diffraction patterns. The data obtained from these films were treated as discussed below. The data from both films were fit by a room-temperature, cubic lattice parameter of 4.0782 ± 0.0004 A, in excellent agreement with the published values of 4.0781 ± 0.0003 A (18°C)[51] and 4.07864 A (25°C).[52]

E. Data Treatment

In general the line positions on the powder patterns were independently measured by two observers and their results averaged. Lines not measured by both observers were excluded from the line list and the fitting procedure described below. Miller indices were assigned to the observed lines by comparison with available diffraction data on isostructural compounds and through the use of $\sin^2\theta$ and theoretical line intensity calculations, performed by the POWD program developed by Smith,[53] or the ANIFAC program developed by Larson, Roof, and Cromer.[54] Following

indexing the observed angles were transferred to cards for computer determination of the most probable lattice parameters according to a least squares fit of the differences between observed and calculated $\sin^2\theta$ values, as carried out by the LCR-2 program developed by Williams.[55] This program weights each observed line by a factor proportional to $1/\sin^2(2\theta_i)\sigma^2(\theta_i)$, where $\sigma(\theta_i)$ is the random error in the measurement of θ_i. A value of 0.05° was assigned to $\sigma(\theta_i)$, in accordance with the film reader precision. When an experimentally observed line was considered to be composed of two or more theoretically possible lines, each of these lines was assigned a $\sigma(\theta_i)$ value proportional to its theoretically calculated intensity, with the condition that the $\sigma(\theta_i)$ value for the entire group of lines remained equal to 0.05°. This procedure prevented "overweighting" of observed lines when they were composed of more than one component. No extrapolation functions were used in the least squares routine, since the use of precision x-ray cameras and very small samples essentially eliminates errors due to sample eccentricity and absorption.[29]

Unless otherwise stated, all reported lattice parameter error limits represent the 95% confidence range (equal to 2σ) reflecting only the internal consistency of the data for that particular preparation. Multiple preparations of each compound type were carried out in order to achieve some degree of statistical sampling.

V. CRYSTALLOGRAPHIC RESULTS

The crystal structures and lattice parameters of the compounds of berkelium prepared in this work are discussed in this section. Comparisons of the berkelium crystallographic results with those of similar lanthanide and actinide compounds are made where appropriate.

A. Berkelium Dioxide and Cubic Berkelium Sesquioxide

The first sample of berkelium dioxide was prepared by Cunningham and Wallmann in 1962.[18] They reported a lattice parameter of 5.33 ± 0.02 A based on the indexing of four lines in the face-centered cubic, fluorite-type structure, obtained from 0.004 μg of berkelium dioxide.

Many samples of berkelium dioxide and several of cubic berkelium sesquioxide were prepared during the course of this work. All of the berkelium dioxide samples exhibited the fluorite-type, face-centered cubic structure. The observed lattice parameters of a few of the individual compound preparations, along with their Cf^{249} content and method of preparation, are listed in Table V-1.

Note that in the case of the berkelium dioxides the cubic parameter increases with time, apparently corresponding to the formation of the larger-than-Bk^{4+} Cf^{3+} ions; however, the oxidation state assumed by Cf in a BkO_2 matrix is not known. The opposite case is evident in the sesquioxides, since Cf^{3+} is smaller than Bk^{3+}.

The change in the cubic lattice parameter of BkO_2 with time was studied and found to increase about one percent over the 178 days of observation. Unfortunately, the dioxide sample used for this study contained 9.53 atom percent cerium. The lattice parameter increased regularly over the first 15 days of observation. At that time the sample was annealed in its quartz capillary at ~600°C for 90 min. The cubic lattice parameter derived from the annealed sample was eight-tenths percent greater than the parameter of the dioxide sample before the annealing treatment. The dioxide parameter remained at this value (within the lattice parameter 2σ error limits) over the next 163 days. No further annealing treatments were carried out. This abnormal behavior is probably linked with the presence of the Cf^{3+} ions in the crystal, growing in from the decay of Bk at

Table V-1. Crystallographic properties of the berkelium oxides.

Sample Number	Film Number	Compound[a]	Cf^{249}[b] Content (atom %)	Observed[c] a_o (A)	$\pm 2\sigma$[d]	Method of Preparation
JRP-VIII	2560A	BkO_2	0.88	5.334	0.001	air ignition at 1200°C
JRP-X	2564A	BkO_2	1.10	5.335	0.001	$Bk_2O_3 + O_2$ at 600°C for 61 min
JRP-XVII	2596A	BkO_2	3.68	5.336	0.001	air-fired BkO_2 + HF at 500°C for 62 min
JRP-X	2568A	Bk_2O_3	1.53	10.889	0.003	low-temp. BkO_2 + H_2 at 600°C for 60 min
JRP-IX	2572A	Bk_2O_3	1.75	10.887	0.001	H_2 reduction of higher oxide at 600°C for 64 min
JRP-XV	2590A	Bk_2O_3	3.26	10.885	0.001	air fired BkO_2 + H_2 at 600°C for 60 min

[a] The stoichiometries of both berkelium oxides were assumed. Direct determination was deemed impossible on the 0.2 μg samples.

[b] Calculated assuming Bk^{249} half life is 314 days. Other known contaminants: 0.27 atom percent Ce, 0.06 atom percent Nd.

[c] Calculated least squares value using the LCR-2 program.[55]

[d] This represents the 95% confidence range reflecting only the internal consistency of the data for the individual preparation.

a rate of ~0.2 percent per day. As cubic CeO_2 undoubtedly formed a solid solution with the BkO_2, its presence in the sample only affected the absolute value of the cubic lattice parameter observed, since the amount of cerium remained constant over the period of observation.

The Miller indices, line list, calculated 2θ values, and the observed and calculated line intensities for a representative BkO_2 pattern are given in Table V-2. All observed lines could be indexed on the basis of the assumed, CaF_2 (fluorite) structure, and the agreement between observed and calculated line intensities was considered good.

A plot of the cubic lattice parameters of the actinide "dioxides" is shown in Fig. V-1. Dioxides of elements beyond berkelium are unknown. Although the data clearly show the "actinide contraction", the evident cusp at Cm has no immediate explanation. The similar cusp noted in sesquioxide parameters of the 4f elements has been attributed to the effect of the half-filled, 4f subshell. In the actinide dioxides, however, this point should appear at Bk rather than Cm. An alternative explanation is that the oxygen-curium ratio in "CmO_2" is substantially below 2, or the oxygen-berkelium ratio in "BkO_2" is greater than 2.

Assuming that the actinide "dioxides" do in fact have that stoichiometry, a self-consistent set of actinide quadrivalent ionic radii can be calculated from the dioxide unit cell parameters. Adopting the conventions of Zachariasen,[56] whereby 0.10 A is added to correct the metal-oxygen distance for covalent character in the metal-oxygen bond, the O^{2-} ionic radius is taken to be 1.46 A, and 0.08 A is subtracted to correct from coordination number 8 to 6, the following quadrivalent ionic radii in angstroms were calculated:

Th^{4+}	0.984	Pu^{4+}	0.896
Pa^{4+}	0.944	Am^{4+}	0.888
U^{4+}	0.929	Cm^{4+}	0.886
Np^{4+}	0.913	Bk^{4+}	0.870

Table V-2. Line list and indexing for BkO_2 (JRP-VIII, Film 2560A).

hkl	2θ (deg)		Line Intensity	
	Observed[a]	Calculated[b]	Observed[a]	Calculated[c]
111	28.99	29.00	10.0	10.0
200	33.60	33.61	6.5	3.8
220	48.25	48.26	8.5	4.8
311	57.24	57.29	8.5	4.7
222	60.09	60.09	4.0	1.1
400_{α_1}	70.54	70.57	3.5	0.8
331_{α_1}	78.04	78.03	5.5	2.0
420_{α_1}	80.49	80.46	4.5	1.5
422_{α_1}	90.08	90.07	5.5	1.7
333_{α_1}	97.33	97.25	5.5	1.8
440_{α_1}	109.54	109.56	3.0	0.8
531_{α_1}	117.38	117.39	5.5	1.8
531_{α_2}	117.83	117.86	3.5	0.9
600_{α_1}	120.08	120.11	4.5	1.0
600_{α_2}	120.63	120.61	2.5	0.5
620_{α_1}	131.93	131.96	5.5	1.3
620_{α_2}	132.63	132.60	3.5	0.6
533_{α_1}	142.58	142.53	5.0	1.4
533_{α_2}	143.43	143.38	3.5	0.7
622_{α_1}	146.63	146.66	5.0	1.4
622_{α_2}	147.57	147.62	3.5	0.7

[a] Two independent observers' averaged readings (2θ readings are ± 0.10°) and averaged intensities on a scale from 10 to 0.

[b] Based on the cubic parameter 5.3335 A, $\lambda(\bar{\alpha})$ = 1.54178 A, $\lambda(\alpha_1)$ = 1.54051 A, and $\lambda(\alpha_2)$ = 1.54433 A.

[c] Calculated using the POWD intensity program[53] and scaled such that the most intense line had I ≈ 10.

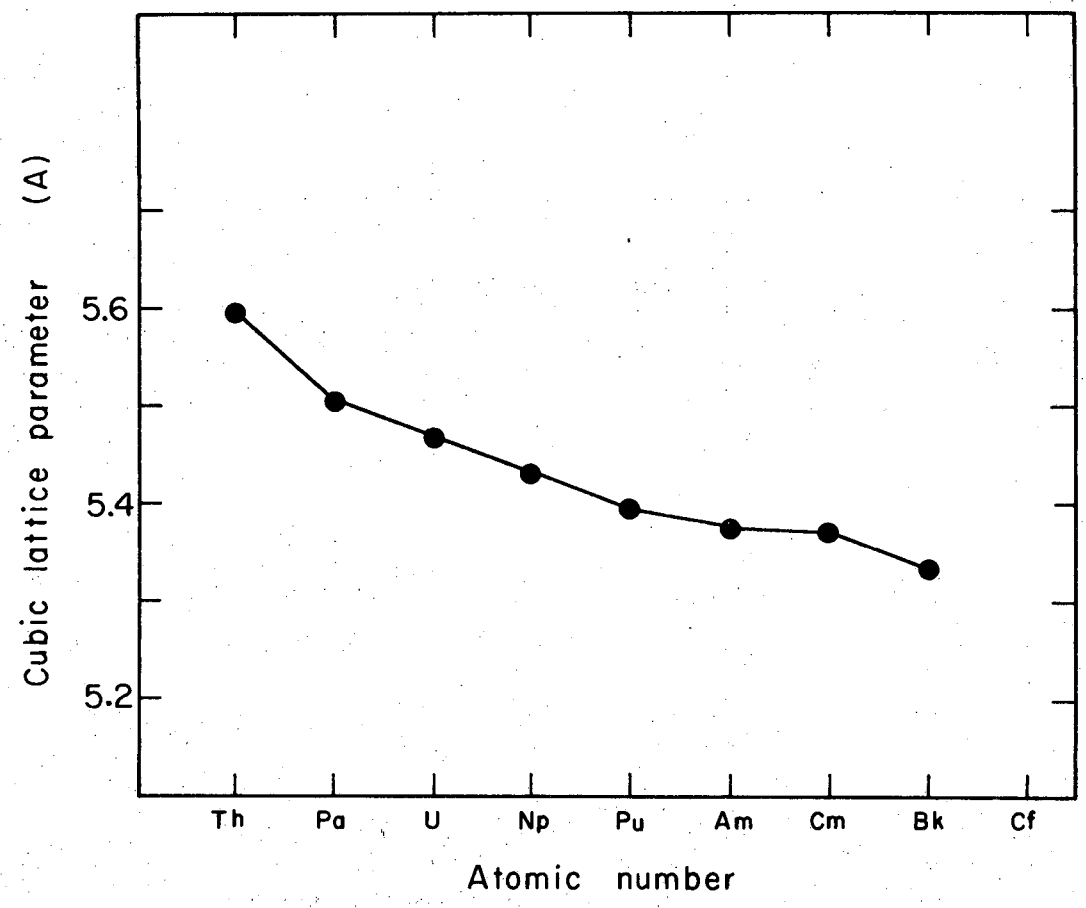

XBL675-3149

Fig. V-1. Actinide dioxide lattice parameters.

The assumptions made in calculating these numbers should be borne in mind. At best, they are relative values and in many instances were calculated from cubic parameters derived from oxides whose exact stoichiometries have not been determined. However, the numbers clearly reflect an "actinide contraction".

The Miller indices, line list, calculated 2θ values, and the observed and calculated line intensities for one of the samples of cubic berkelium sesquioxide are given in Table V-3. All lines could be indexed on the basis of the assumed $(Fe,Mn)_2O_3$, bixbyite, structure[57], and the agreement between observed and calculated line intensities was considered satisfactory.

A plot of the cubic lattice parameters of the lanthanide and actinide Mn_2O_3-type sesquioxides is shown in Fig. V-2. The lattice parameter of Cf_2O_3 plotted here is from the average of two samples prepared recently by Copeland.[58] Both series of sesquioxides show the characteristic 4f and 5f contractions, as well as the cusp at the point of the half-filled, electron subshell.

This series of isomorphic compounds lends itself for calculation of the corresponding trivalent ionic radii. Following the method of Zachariasen,[56] the six-fold coordinated, trivalent ionic radii were calculated to be as tabulated in Table V-4. The numbers given in Table V-4 should be regarded with caution and considered only as relative values. Such relative values are often very useful, however, for predicting actinide crystal chemistry on the basis of radius ratios and known lanthanide crystal chemistry. They are also useful in the correlation of various thermodynamic properties.

Table V-3. Line list and indexing for Bk_2O_3 (JRP-IX, Film 2572A).

hkl	2θ (deg)		Line Intensity	
	Observed[a]	Calculated[b]	Observed[a]	Calculated[c]
222	28.40	28.40	10	10.0
321	30.80	30.73	0-1	0.3
400	32.90	32.91	8	4.0
411	34.92	34.97	2-3	0.5
332	38.72	38.80	1	0.2
431	42.32	42.33	6	0.7
125	45.52	45.64	0-1	0.2
440	47.22	47.23	9	3.9
433	48.82	48.77	1	0.2
600	50.22	50.28	1	0.04
611	51.82	51.76	3	0.5
541	54.52	54.63	2	0.4
622	56.02	56.03	8	3.6
631	57.34	57.41	4	0.6
444	58.84	58.76	4	0.8
543	60.04	60.09	2	0.2
640	61.34	61.41	1	0.1
633	62.74	62.71	1-2	0.3
642	64.04	64.00	4	0.1
156	67.74	67.78	2	0.3
800	69.04	69.01	3	0.5
811	70.24	70.24	2	0.4
820	71.54	71.45	1	0.2
653	72.64	72.66	2	0.2
822	73.84	73.86	2	0.1
831	75.04	75.06	3	0.4
662	76.24	76.24	6	1.1
840	78.54	78.60	6	0.9
833	79.66	79.77	0-1	0.1
842	81.06	80.93	0-1	0.1

Table V-3 (continued)

hkl	2θ (deg)		Line Intensity	
	Observed[a]	Calculated[b]	Observed[a]	Calculated[c]
655	82.16	82.09	2	0.3
851	84.36	84.41	3	0.3
763	86.76	86.71	2-3	0.2
844	87.86	87.86	5	0.7
853_{α_1}	88.86	88.92	3	0.3
860_{α_1}	89.96	90.07	0-1	0.2
1011_{α_1}	91.16	91.22	0-1	0.1
862_{α_1}	92.36	92.36	3	0.4
1022_{α_1}	94.66	94.66	5-6	0.8
765_{α_1}	95.76	95.82	3-4	0.4
855_{α_1}	98.16	98.13	3	0.3
864_{α_1}	99.26	99.29	2-3	0.3
1033_{α_1}	100.56	100.45	2	0.2
1042_{α_1}	101.76	101.62	0-1	0.3
873_{α_1}	102.98	102.80	1-2	0.3
1051_{α_1}	105.16	105.16	3	0.3
880_{α_1}	106.38	106.35	2-3	0.2
1053_{α_1}	109.88	109.98	3	0.3
875_{α_1}	112.48	112.44	0-1	0.3
1062_{α_1}	113.68	113.68	4-5	0.7
884_{α_1}	116.18	116.21	3	0.4
981_{α_1}	117.38	117.50	2-3	0.4
1220_{α_1}	118.78	118.80	0-1	0.3
1071_{α_1}	120.08	120.12	0-1	0.3
1222_{α_1}	121.28	121.46	0-1	0.4
983_{α_1}	122.78	122.81	1-2	0.3
1161_{α_1}	125.50	125.58	2	0.4
1240_{α_1}	127.00	127.01	2	0.5
1242_{α_1}	129.80	129.94	2	0.7
976_{α_1}	131.40	131.45	0-1	0.3

Table V-3 (continued)

hkl	2θ (deg)		Line Intensity	
	Observed[a]	Calculated[b]	Observed[a]	Calculated[c]
1082_{α_1}	132.90	133.00	2	0.5
985_{α_1}	134.60	134.59	2	0.4
1066_{α_1}	136.30	136.23	1	0.2
1066_{α_2}	137.00	136.94	0-1	0.1
1075_{α_1}	137.90	137.91	1	0.3
1244_{α_1}	139.60	139.65	1	0.4
1253_{α_1}	141.50	141.46	0-1	0.2
1260_{α_1}	143.40	143.34	3	1.1
1091_{α_1}	145.20	145.31	1-2	0.5
1262_{α_1}	147.30	147.38	2	1.0
1181_{α_1}	149.62	149.57	1-2	0.7
1093_{α_1}	154.62	154.46	2-3	0.4
987_{α_1}	160.42	160.45	3	1.2
987_{α_2}	162.32	162.17	1-2	0.6
1264_{α_1}	164.22	164.23	2-3	1.9

[a] A single reading of the powder pattern (2θ readings are ± 0.10°). Observed intensities are on a scale of 10 to 0.

[b] Based on the cubic parameter 10.8865 A, $\lambda(\bar{\alpha})$ = 1.54178 A, $\lambda(\alpha_1)$ = 1.54051 A, $\lambda(\alpha_2)$ = 1.54433 A.

[c] Calculated using the POWD intensity program[53] and scaled such that the most intense line had I = 10.0.

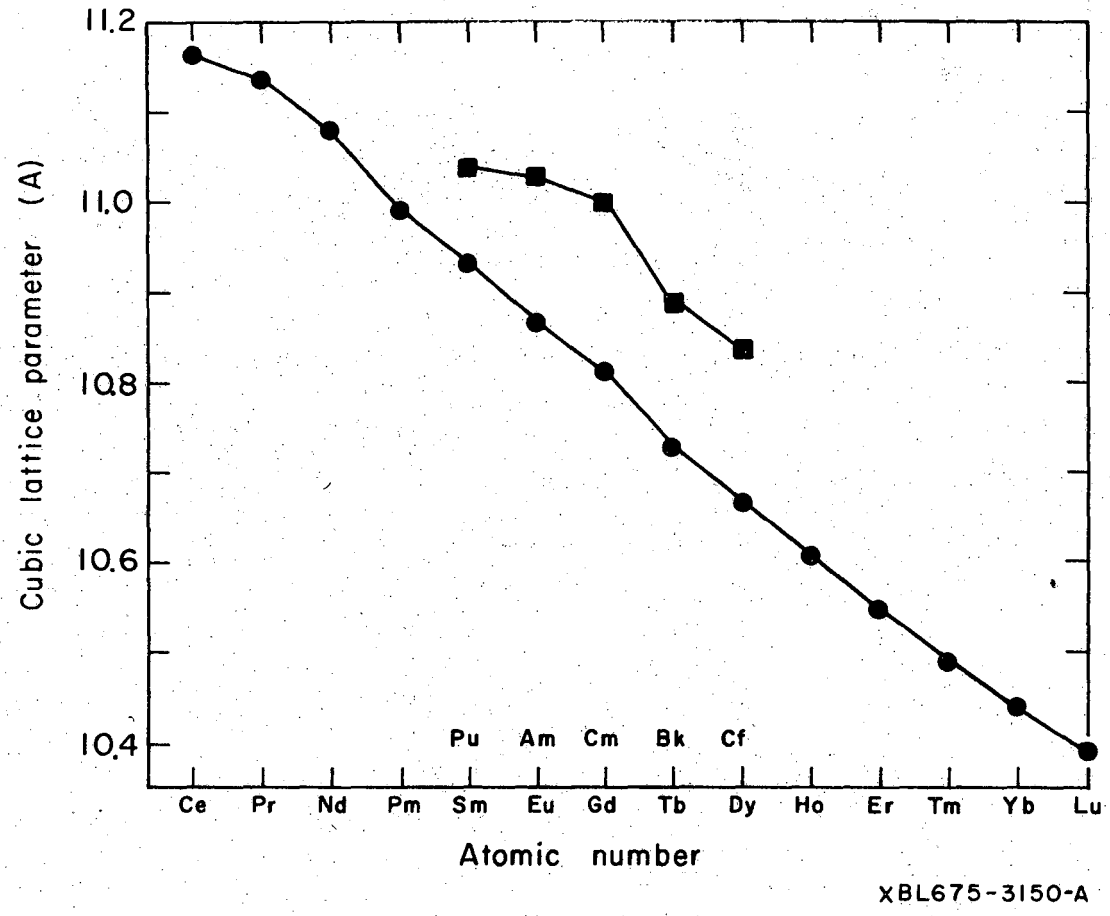

Fig. V-2. Cubic lattice parameters of the lanthanide and actinide Mn_2O_3-type sesquioxides.

Table V-4. Ionic radii[a] of the trivalent lanthanide[59] and actinide ions (CN=6).

Ion	Radius, A	Ion	Radius, A	Ion	Radius, A
Ce^{+++}	1.018	Tb^{+++}	0.920	Pu^{+++}	0.987
Pr^{+++}	1.008	Dy^{+++}	0.907	Am^{+++}	0.985
Nd^{+++}	0.995	Ho^{+++}	0.894	Cm^{+++}	0.979
Pm^{+++}	0.976	Er^{+++}	0.881	Bk^{+++}	0.954
Sm^{+++}	0.964	Tm^{+++}	0.869	Cf^{+++}	0.944
Eu^{+++}	0.950	Yb^{+++}	0.858		
Gd^{+++}	0.938	Lu^{+++}	0.848		

[a]Calculated according to the following formula:

Ionic Radius = $0.21441(a_o) - 1.46 + 0.08$

where a_o is the cubic sesquioxide lattice parameter, 1.46 A is taken to be the O^{2-} radius,[56] and 0.08 A is assumed to be the correction for covalent character in the metal-oxygen bond.[56]

B. Berkelium Trichloride

All $BkCl_3$ samples prepared exhibited the UCl_3-type hexagonal structure. The observed lattice parameters of the individual trichloride preparations along with their Cf^{249} content are listed in Table V-5. Films 2587A and 2598A showed pure trichloride phases, whereas Film 2600A showed mixed phases of $BkCl_3$ and BkOCl, predominantly the former. Film 2652A was a second exposure of sample number JRP-XVI (Film 2598A), after an 85-day time lapse. This was to see if the lattice parameters would shift noticeably toward those of $CfCl_3$ as the Cf^{249} content in the $BkCl_3$ increased. Comparison with the UCl_3-type hexagonal $CfCl_3$ lattice parameters,[27,61] $a_o = 7.393 \pm 0.040$ A and $c_o = 4.090 \pm 0.060$ A, clearly shows the expected expansion in the a_o parameter and shrinkage in the c_o parameter.

In accordance with Vegard's Law[60] (assuming ideal homogeneous solid solutions), the observed lattice parameters were corrected for the known Cf and Ce contents (0.27 atom %), then averaged to obtain "best estimates" for the lattice parameters of $BkCl_3$: $a_o = 7.382 \pm 0.002$ A, $c_o = 4.127 \pm 0.003$ A. The error limits placed on these average lattice parameter values were computed using the 95% confidence level, equal to $(4.30/\sqrt{N})\sqrt{\Sigma d_i^2)/(N-1)}$, where d_i is the deviation of the individual lattice parameters from the average value, N is the number of observations, and the factor 4.30 is the 95% confidence Student t value for three observations.

The Miller indices, line list, calculated 2θ values, and the observed and calculated line intensities for one of the $BkCl_3$ samples are given in Table V-6.

Plots of the a_o and c_o lattice parameters of the UCl_3-type actinide trichlorides are given in Figs. V-3(a) and V-3(b), respectively. These plots show that, in the case of the actinide trichlorides, the "actinide contraction" is clearly anisotropic.

Usually such a series of isomorphic compounds lends itself for calculation of the corresponding ionic radii; however, because of the anisotropies in this trichloride series, the concept of ionic radius should be regarded with considerable caution. Radii calculations are based on averaged interatomic distances; and the radius concept begins to lose meaning when the distances averaged are considerably different.

Table V-5. Berkelium trichloride lattice parameters (UCl_3-type hexagonal).

Sample Number	Film Number	Cf^{249}[a] Content (atom %)	Observed Lattice Parameters[b] (A) $a_o \pm 2\sigma$	$c_o \pm 2\sigma$
JRP-XIV	2587A	3.04	7.382 ± 0.001	4.127 ± 0.001
JRP-XVI	2598A	3.68	7.384 ± 0.001	4.127 ± 0.001
JRP-XVII	2600A	3.90	7.383 ± 0.001	4.125 ± 0.001
JRP-XVI	2652A	20.17	7.387 ± 0.001	4.122 ± 0.001

[a] Calculated assuming Bk^{249} half life is 314 days. Other known contaminants: 0.27 atom percent Ce, 0.06 atom percent Nd.

[b] Lattice parameters are the least squares value. The 2σ error limits represent the 95% confidence range reflecting only the internal consistency of the data for the individual preparation.

Table V-6. Line list and indexing for $BkCl_3$ (JRP-XIV, Film 2587A).

hkl	2θ (deg)		Line Intensity	
	Observed[a]	Calculated[b]	Observed[a]	Calculated[c]
110	24.09	24.11	9.0	6.8
101	25.68	25.69	9.5	10.0
200	27.93	27.91	5.0	2.3
111	32.58	32.54	3.3	1.1
201	35.48	35.52	9.7	9.2
210	37.23	37.21	4.5	1.6
300	42.37	42.42	7.0	3.6
211	43.32	43.39	9.0	7.7
002	43.92	43.87	2.7	1.5
102	46.32	46.22	3.5	1.0
220	49.37	49.38	3.3	1.4
112	50.62	50.68	5.5	2.1
310	51.52	51.54	2.5	0.8
202	52.82	52.80	2.8	0.8
131	56.53	56.49	5.5	2.3
400	57.72	57.68	1.5	0.4
212	58.87	58.85	3.8	0.9
401	62.27	62.30	1.3	0.7
302	62.72	62.67	5.5	2.2
230	63.42	63.42	0.7	0.5
410	67.07	67.09	4.0	1.3
231	67.87	67.81	6.0 broad	2.8
222		68.17		1.1

Table V-6 (continued)

hkl	2θ (deg)		Line Intensity	
	Observed[a]	Calculated[b]	Observed[a]	Calculated[c]
103	69.97	69.94	4.3	0.7
312		69.95		0.7
203	75.21	75.18	4.5	1.0
402		75.19		0.4
501	78.21	78.28	2.0	1.0
213	80.31	80.30	4.8	1.4
232		80.31		0.5
421	83.34	83.34	5.0	1.1
412	83.64	83.67	5.5	1.5
511	88.36	88.36	4.5	1.2
313	90.30	90.34	4.0	0.7
502		90.35		0.3
332	93.71	93.69	1.0	0.6
403	95.46	95.35	1.0	0.3
242		95.36		0.1
601	96.76	96.71	1.3	0.04
004		96.68		0.2
431_{α_1}	98.26	98.28	2.5 broad	0.8
104_{α_1}		98.25		0.2
512_{α_1}	100.26	100.29	4.8	0.1
323_{α_1}		100.28		0.8
512_{α_2}	100.66	100.64	2.5	0.06
323_{α_2}		100.63		0.4

Table V-6 (continued)

hkl	2θ (deg)		Line Intensity	
	Observed[a]	Calculated[b]	Observed[a]	Calculated[c]
$11\bar{4}\alpha_1$	101.91	101.63	1.8 broad	0.3
$21\bar{4}\alpha_1$	108.56	108.52	3.5	0.2
$16\bar{1}\alpha_1$		108.55		0.6
$60\bar{2}\alpha_1$	109.06	108.90	3.5	0.3
$50\bar{3}\alpha_1$	110.80	110.66	3.5	0.4
$43\bar{2}\alpha_1$		110.67		0.3
$50\bar{3}\alpha_2$	111.10	111.07	2.0	0.2
$43\bar{2}\alpha_2$		111.08		0.2
$30\bar{4}\alpha_1$	112.10	112.07	3.5	0.5
$30\bar{4}\alpha_2$	112.60	112.49	2.0	0.3
$25\bar{2}\alpha_1$	114.25	114.27	3.5	0.9
$42\bar{3}\alpha_1$	116.05	116.09	3.5	0.6
$42\bar{3}\alpha_2$	116.55	116.55	1.8	0.3
$22\bar{4}\alpha_1$	117.60	117.57	1.8	0.4
$22\bar{4}\alpha_2$	118.20	118.04	1.0	0.2
$70\bar{1}\alpha_1$	119.40	119.50	3.5	0.3
$53\bar{1}\alpha_1$		119.50		0.7
$31\bar{4}\alpha_1$		119.47		0.2
$51\bar{3}\alpha_1$	121.80	121.80	4.0	0.8
$61\bar{2}\alpha_1$		121.81		0.2
$51\bar{3}\alpha_2$	122.40	122.31	2.0	0.4
$61\bar{2}\alpha_2$		122.32		0.1

Table V-6 (continued)

hkl	2θ (deg) Observed[a]	2θ (deg) Calculated[b]	Line Intensity Observed[a]	Line Intensity Calculated[c]
404_{α_1}	125.39	125.38	3.5 broad	0.2
621_{α_1}		125.41		0.7
710_{α_1}	130.90	130.92	1.5	0.6
324_{α_1}	131.80	131.77	1.5	0.3
442_{α_1}	132.30	132.24	2.0	0.6
433_{α_1}	134.50	134.52	3.5	0.7
702_{α_1}		134.53		0.2
532_{α_1}		134.53		0.4
433_{α_2}	135.20	135.20	2.0	0.4
702_{α_2}		135.22		0.09
532_{α_2}		135.22		0.2
414_{α_1}	136.30	136.40	4.3	1.1
414_{α_2}	137.15	137.12	2.0	0.6
450_{α_1}	140.39	140.46	1.3	0.05
105_{α_1}		140.39		0.4
262_{α_1}	142.04	142.04	1.3	0.4
541_{α_1}	147.29	147.22	3.0	1.1
504_{α_1}		147.17		0.3
800_{α_1}	149.09	149.12	2.5	0.1
205_{α_1}		149.03		0.8
800_{α_2}	149.94	150.17	1.3	0.05
205_{α_2}		150.08		0.4
163_{α_1}	151.09	151.09	4.0	1.2

Table V-6 (continued)

hkl	2θ (deg)		Line Intensity	
	Observed[a]	Calculated[b]	Observed[a]	Calculated[c]
163_{α_2}	152.19	152.21	1.8	0.6
334_{α_1}	153.99	153.95	2.5 broad	0.8
334_{α_2}	154.99	155.21	1.5 broad	0.4
712_{α_1}	158.98	159.01	4.0 broad	2.9
712_{α_2}	160.73	160.60	4.0 broad	1.6
215_{α_1}		160.83		2.1

[a] Two independent observers' averaged readings (2θ readings are ± 0.10°) and averaged intensities on a scale from 10 to 0.

[b] Based on the hexagonal lattice parameters a_o = 7.3817 A, c_o = 4.1274 A and $\lambda(\bar{\alpha})$ = 1.54178 A, $\lambda(\alpha_1)$ = 1.54051 A, and $\lambda(\alpha_2)$ = 1.54433 A.

[c] Calculated using the POWD program,[53] assuming the atomic coordinates of UCl_3[62] for those of $BkCl_3$, and scaled such that the most intense line had I = 10.0.

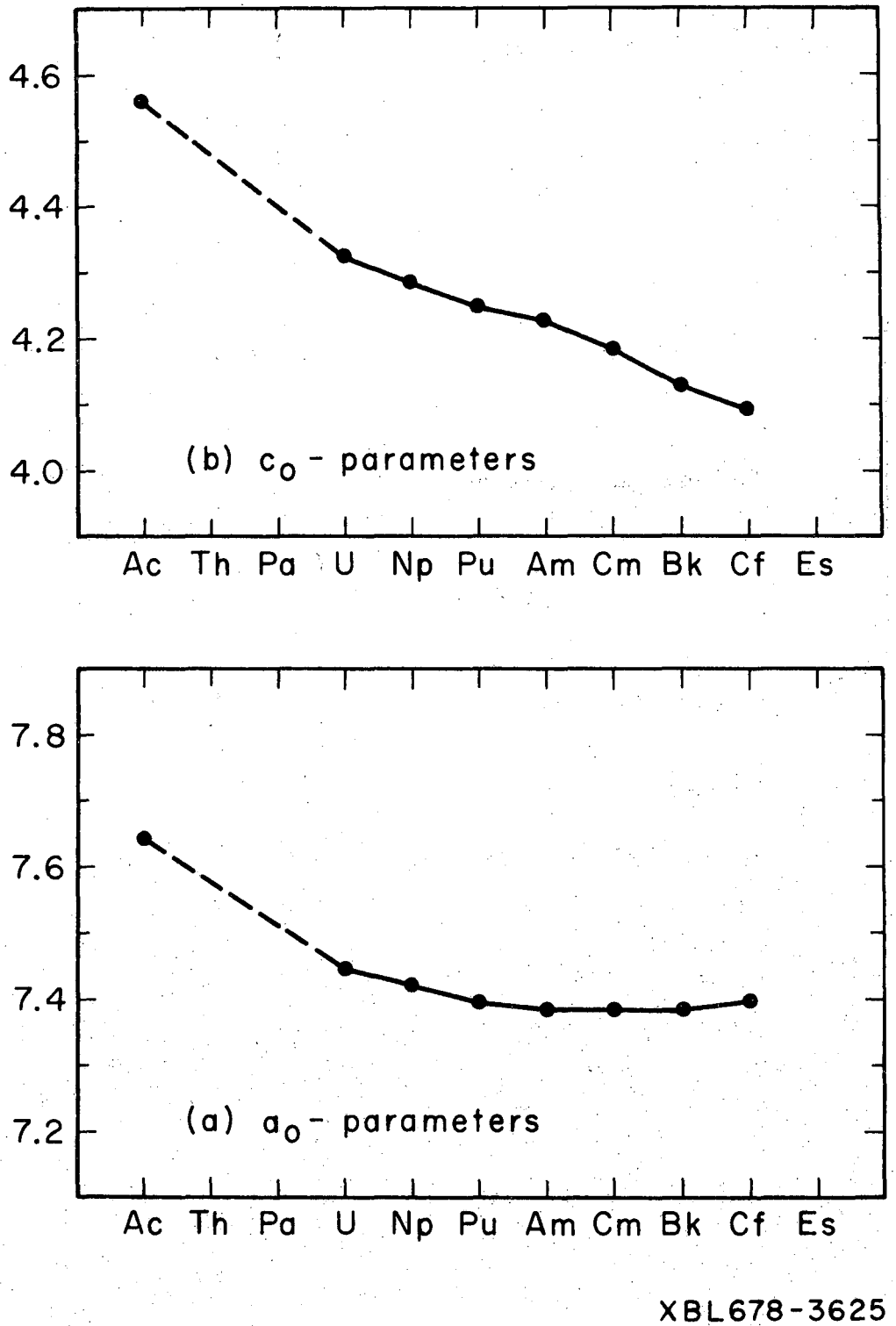

Fig. V-3. Lattice parameters in angstroms of the UCl_3-type hexagonal actinide trichlorides.

The M-Cl bond distances in the UCl_3-type actinide trichlorides and calculated trivalent ionic radii are listed in Table V-7. Calculations similar to those presented in Table V-7 show that the lanthanide trichlorides also exhibit an anisotropic "lanthanide contraction". Comparison of the similarly calculated trivalent ionic radii shows almost identical values for the following lanthanide-actinide pairs: Gd-Cf, Eu-Bk, Sm-Cm, Pm-Am, Nd-Pu, Pr-Np and Ce-U.

Because of the extreme anion crowding in the UCl_3-type trichloride structure and by analogy with the lanthanide trichlorides, it is very probable that there will be a crystal structure change noted in the actinide trichlorides heavier than $CfCl_3$. In the corresponding lanthanide trichloride series, the crystal structure changes from the UCl_3-type hexagonal (Ce-Gd)[63] to the $PuBr_3$-type orthorhombic (Tb)[64] to the YCl_3-type monoclinic (Dy-Lu).[65] The realization of this prediction will have to wait until $EsCl_3$ is prepared and its crystal structure is determined.

C. Berkelium Oxychloride

Unlike berkelium trichloride, berkelium oxychloride is not hygroscopic. All BkOCl samples prepared were found to exhibit the PbFCl-type tetragonal structure.[66] In general the BkOCl powder patterns were of poorer quality than those obtained from other berkelium compounds, in that the high-angle lines were often light and diffuse.

The observed lattice parameters of three individual oxychloride preparations along with their Cf^{249} content are listed in Table V-8. Film 2600A showed mixed phases of $BkCl_3$ and BkOCl; film 2610A showed the BkOCl pattern plus a few weak, unaccounted-for lines (perhaps due to impurities on the outside of the x-ray capillary); and film 2612A showed only the BkOCl pattern.

Table V-7. Actinide-chloride bond distances and actinide trivalent ionic radii (derived from UCl_3-type hexagonal actinide trichloride crystal data).

Actinide Trichloride	Lattice Parameters (A) a_o	c_o	M-Cl Bond Distances (A) apical	equitorial	Ionic Radius[a] (A) (CN = 6)
Ac	7.64	4.56	3.092	3.036	1.153
U	7.443	4.321	2.968	2.958	1.045
Np	7.420	4.282	2.949	2.948	1.029
Pu	7.395	4.246	2.931	2.939	1.014
Am	7.384	4.225	2.922	2.934	1.006
Cm	7.380	4.185	2.907	2.933	0.996
Bk	7.382	4.127	2.886	2.933	0.982
Cf	7.393 7.40	4.090 4.070	2.875	2.938	0.976

[a]Calculated according to the following formula:

Ionic Radius = [3(M-Cl equitorial bond distance) + 6(M-Cl apical bond distance)]/9 - 1.81 - 0.11

where the chloride ionic radius is taken to be 1.81 A[56] and the 9-fold to 6-fold coordination correction number is taken to be 0.11 A.[56]

Table V-8. Berkelium oxychloride lattice parameters (PbFCl-type tetragonal).

Sample Number	Film Number	Cf^{249} Content[a] (atom %)	Observed Lattice Parameters[b] (A)	
			$a_o \pm 2\sigma$	$c_o \pm 2\sigma$
JRP-XVII	2600A	3.90	3.964 ± 0.003	6.709 ± 0.005
JRP-XVII	2610A	4.95	3.967 ± 0.001	6.711 ± 0.003
JRP-XX	2612A	5.16	3.965 ± 0.001	6.704 ± 0.003

[a] Calculated assuming Bk^{249} half life is 314 days. Other known contaminants: 0.27 atom percent Ce, 0.06 atom percent Nd.

[b] Lattice parameters are the least squares value. The 2σ error limits represent the 95% confidence range reflecting only the internal consistency of the data for the individual preparation.

The three sets of lattice parameters were corrected for the known Ce and Cf contents, by assuming that the impurities formed ideal solid oxychloride solutions with the berkelium (Vergard's Law). The CeOCl parameters used were those of Templeton and Dauben:[67] $a_o = 4.080 \pm 0.004$ A and $c_o = 6.831 \pm 0.007$ A; the CfOCl parameters, recently determined by Copeland,[58] are $a_o = 3.956 \pm 0.002$ A and $c_o = 6.662 \pm 0.009$ A. These "corrected", BkOCl parameters were then averaged to obtain "best estimates" for the lattice parameters of BkOCl: $a_o = 3.966 \pm 0.004$ A and $c_o = 6.710 \pm 0.009$ A, where the error limits are the 95% confidence interval calculated using the standard statistical method for the average of three independent determinations.

The Miller indices, line list, calculated 2θ values, and the observed and calculated line intensities for one of the BkOCl samples are given in Table V-9.

There are relatively few data in the literature dealing with the oxychlorides of the actinides. All of the known actinide oxychlorides, as well as the oxychlorides of La through Er (PmOCl is unknown), exhibit the PbFCl-type tetragonal structure. The remaining three lanthanides exhibit an oxychloride structure whose type has not been determined. ErOCl is bimorphic.

A plot of the molecular volumes (Z = 2) of the PbFCl-type actinide and lanthanide oxychlorides is shown in Fig. V-4. With the exception of UOCl[69] the correlation is good, showing the familiar contractions in the lanthanide and actinide series.

The calculated density (x-ray) of BkOCl is 9.45 g/cc.

Similar to the UCl_3-type actinide trichlorides, the anion crowding is very severe in this PbFCl-type tetragonal structure. In BkOCl the oxygen-oxygen distance is 2.80 A, the chlorine-chlorine distance 3.34 A. The berkelium-oxygen distance is 2.32 A, whereas the berkelium-chlorine distances are 3.07 A (four nearest neighbors) and 3.05 A (one nearest neighbor). Both anion-anion distances are considerably smaller than twice the crystal radii given by Zachariasen for O^{2-} (1.46 A) and Cl^- (1.81 A).[56] Different values are obtained for the Bk^{3+} radius from the berkelium-chlorine and berkelium-oxygen distances. These calculations clearly illustrate the limitations of the ionic radius concept.

Table V-9. Line list and indexing for BkOCl (JRP-XX, Film 2612A).

hkl	2θ (deg)		Line Intensity	
	Observed[a]	Calculated[b]	Observed[a]	Calculated[c]
101	26.10	26.11	10.0	10.0
110	31.89	31.92	9.0	5.8
102	35.04	35.05	9.5	6.6
003	40.34	40.36	2.0	0.8
112	41.94	42.01	5.5	2.5
200	45.73	45.76	6.5	2.7
201	47.78	47.84	2.5	0.5
113	52.23	52.35	4.5	2.2
211	53.43	53.45	6.5	3.1
202		53.71		0.8
212	58.83	58.92	6.0	2.9
104	59.83	59.92	3.8	1.8
203	62.53	62.64	3.5	1.0
220	66.67	66.72	3.5	0.9
301	73.03	72.95	3.5	0.6
222		73.18		0.4
310	75.88	75.87	3.5	1.0
311	77.63	77.43	1.8	0.2
302		77.65		0.7
214	78.43	78.53	3.0	1.7
223	80.88	80.95	2.0	0.5
312	82.02	82.05	2.0	0.7
313	89.77	89.65	2.8	1.0

Table V-9 (continued)

hkl	2θ (deg) Observed[a]	2θ (deg) Calculated[b]	Line Intensity Observed[a]	Line Intensity Calculated[c]
321 α_1	90.42	90.43	2.0	0.5
215 α_1	92.17	92.15	1.3 broad	0.2
322 α_1	94.97	94.98	2.5	0.6
116 α_1	95.77	95.82	2.5	0.3
304 α_1		95.84		0.4
400 α_1	102.01	101.98	1.5 broad	0.2
206 α_1	104.96	104.62	2.0 broad	0.3
225 α_1		105.30		0.3
411 α_1	108.26	108.02	2.5	0.5
402 α_1		108.25		0.1
107 α_1	111.66	111.67	0.5	0.4
412 α_1	112.91	112.87	1.8	0.6
324 α_1	113.81	113.80	1.3	0.8
420 α_1	120.65	120.63	2.3	0.5
226 α_1	123.85	123.66	1.0 broad	0.4
333 α_1	126.75	126.59	1.3 broad	0.3
325 α_1	129.90	129.88	0.8 broad	0.2
217 α_1	132.10	132.15	2.5 broad	1.0
316 α_1	134.85	134.85	3.5	0.8
414 α_1		134.87		1.0
316 α_2	135.54	135.54	2.0	0.4
414 α_2		135.56		0.5

Table V-9 (continued)

hkl	2θ (deg) Observed[a]	2θ (deg) Calculated[b]	Line Intensity Observed[a]	Line Intensity Calculated[c]
423 α_1	138.29	138.34	1.5 broad	0.7
431 α_1	155.88	155.95	2.0 broad	1.9

[a] Two independent observers' averaged readings (2θ values are ± 0.10°) and averaged intensities on a scale from 10 to 0.

[b] Based on the tetragonal lattice parameters a_o = 3.9651 A, c_o = 6.7038 A, and $\lambda(\bar{\alpha})$ = 1.54178 A, $\lambda(\alpha_1)$ = 1.54051 A, and $\lambda(\alpha_2)$ = 1.54433 A.

[c] Calculated using the POWD intensity program,[53] assuming the atomic coordinates of AmOCl[68] for those of BkOCl, and scaled such that the most intense line had I = 10.0.

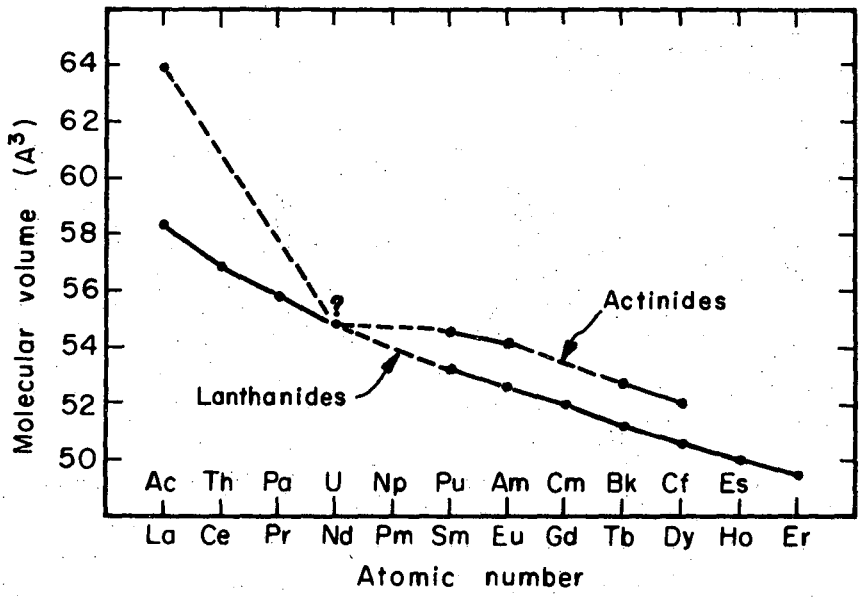

Fig. V-4. Molecular volumes of the PbFCl-type lanthanide and actinide oxychlorides.

D. Berkelium Trifluoride

The results of this work indicate that berkelium trifluoride exhibits two stable crystal structures, the LaF_3-type trigonal structure,[70] characteristic of the lanthanide trifluorides of La through Nd, and the YF_3-type orthorhombic structure,[71] characteristic of the lanthanide trifluorides of Sm through Lu. Weigel[72] has prepared PmF_3 and found it to exhibit the LaF_3-type trigonal structure.

The observed lattice parameters of the individual trifluoride preparations along with their Cf^{249} and total Ce contents are listed in Table V-10.

Since CeF_3 does not exhibit an orthorhombic modification, the YF_3-type berkelium trifluoride lattice parameters were initially corrected for the Cf content of the Bk sample in accordance with Vegard's Law.[60] The lattice parameters of orthorhombic CfF_3 (a_o = 6.653 ± 0.002 A, b_o = 7.041 ± 0.002 A, and c_o = 7.395 ± 0.001 A) were derived from a single preparation by this author and colleagues.[73]

These "corrected-for-Cf", orthorhombic BkF_3 lattice parameters were then plotted versus the total Ce content of the berkelium sample and extrapolated to zero Ce content to obtain "best estimates" for the lattice parameters of orthorhombic BkF_3: a_o = 6.70 ± 0.01 A, b_o = 7.09 ± 0.01 A, and c_o = 4.41 ± 0.01 A, where the lattice parameters are rounded off to the nearest hundredth, and the error limits reflect the uncertainties in the derivation of the lattice parameters.

Similarly for LaF_3-type berkelium trifluoride, since the trigonal modification of CfF_3 is unknown, the lattice parameters were corrected for the known Ce content of the Bk sample using the parameters of Swanson et al. (a_o = 7.112 A and c_o = 7.279 A).[74] These "corrected-for-Ce", trigonal BkF_3 lattice parameters did not vary in any regular fashion as the Cf content of the berkelium sample increased, so they were just averaged to obtain "best estimates" for the lattice parameters of trigonal BkF_3: a_o = 6.97 ± 0.01 A and c_o = 7.14 ± 0.01 A, where again the lattice parameters are rounded off to the nearest hundredth, and the error limits reflect the uncertainties in the derivation of the lattice parameters.

The Miller indices, line lists, calculated 2θ values, and the observed and calculated line intensities for one sample of each type of BkF_3 are given in Tables V-11 and V-12.

Table V-10. Berkelium trifluoride lattice parameters.

Sample Number	Film Number	Structure Type	Cf^{249}[a] Content (atom %)	Total Ce[b] Content (atom %)	Observed Lattice Parameters[c] (A) $a_o \pm 2\sigma$	$b_o \pm 2\sigma$	$c_o \pm 2\sigma$
JRP-XXIII	2624A	YF_3	7.03	0.27	6.695 ± 0.004	7.086 ± 0.004	4.407 ± 0.003
JP-VII	2691A	YF_3	1.53	9.53	6.717 ± 0.015	7.114 ± 0.011	4.409 ± 0.005[d]
JP-X	2713A	YF_3	5.16	9.53	6.716 ± 0.001	7.103 ± 0.001	4.408 ± 0.001
JRP-XXI	2614A	LaF_3	5.26	0.27	6.973 ± 0.002		7.143 ± 0.003
JRP-XXII	2619A	LaF_3	6.20	0.27	6.965 ± 0.003		7.140 ± 0.003
JP-VII	2691A	LaF_3	1.53	9.53	6.990 ± 0.001		7.157 ± 0.001
JP-X	2716A	LaF_3	5.79	9.53	6.990 ± 0.001		7.158 ± 0.002
JP-X	2734A	LaF_3	8.05	9.53	6.988 ± 0.001		7.156 ± 0.002

[a] Calculated assuming Bk^{249} half life is 314 days.

[b] Determined by mass analysis. See Sec. II-C.

[c] Lattice parameters are the least squares value. The 2σ error limits represent the 95% confidence range reflecting only the internal consistency of the data for the individual preparation.

[d] The second phase in a predominantly trigonal BkF_3 powder pattern.

Table V-11. Line list and indexing for YF_3-type orthorhombic BkF_3 (JP-X, Film 2713A).

hkl	2θ (deg)		Line Intensity	
	Observed[a]	Calculated[b]	Observed[a]	Calculated[c]
011	23.67	23.75	6.5	2.0
101	24.12	24.15	9.0	5.7
020	25.02	25.07	9.0	6.3
200	26.47	26.54	1.5	0.1
111	27.27	27.26	10.0	10.0
210	29.37	29.42	10.0	7.6
201	33.51	33.55	3.5	0.4
121	35.06	35.09	9.0	3.1
211	35.90	35.91	3.0	0.1
002	40.85	40.94	6.5	1.1
221	42.25	42.34	6.5	1.4
102	43.14	43.20	4.0	0.4
031		43.38		0.1
112	44.99	45.13	6.5	1.8
301	45.44	45.44	10.0	2.4
131		45.53		3.6
230	46.84	46.95	8.5	3.2
311	47.29	47.30	7.0	1.8
022	48.54	48.61	7.0	1.5
122	50.53	50.60	7.0	1.4
212	51.23	51.21	8.0 broad	2.3
040		51.46		1.2

Table V-11 (continued)

hkl	2θ (deg)		Line Intensity	
	Observed[a]	Calculated[b]	Observed[a]	Calculated[c]
321	52.58	52.59	7.5	2.1
400	54.53	54.66	5.5	0.9
141	57.57	57.62	6.0	1.0
302	58.82	58.79	5.8	0.2
132		58.87		0.6
312	60.37	60.35	7.5	0.7
411		60.42		0.4
331		60.68		0.9
420	61.02	61.04	6.5	1.0
241	62.77	62.84	3.5	0.3
232	64.01	64.03	6.5	1.1
013	64.76	64.78	6.5	0.8
322		64.91		0.3
113	66.31	66.44	3.0	0.3
042	67.65	67.76	4.5	0.5
430	68.45	68.51	1.5	0.1
142	69.35	69.38	3.0	0.4
051		69.52		0.1
203	69.80	69.87	3.0	0.6
402	70.40	70.50	2.5	0.4
123	71.05	70.79	7.0	0.2
341		71.05		1.0
151		71.12		0.7

Table V-11 (continued)

hkl	2θ (deg) Observed[a]	2θ (deg) Calculated[b]	Line Intensity Observed[a]	Line Intensity Calculated[c]
332		72.17		0.2
250	72.15	72.20	5.5	0.6
431		72.23		0.2
511	75.10	75.13	4.0	0.8
223	75.45	75.52	6.0	1.2
422	76.15	76.14	5.0	0.8
033		76.26		0.4
440	78.39	78.38	3.5	0.6
521	79.19	79.29	3.0	0.3
060	81.23	81.26	4.3	0.4
342	81.83	81.88	4.0	0.2
152		81.95		0.3
351	83.63	83.52	3.0	0.4
531		86.10		0.7
161	86.23	86.30	6.5 broad	0.4
252		86.50		0.6
610	88.28	88.40	3.5 broad	0.5
413	89.73	89.75	5.5 broad	0.8
522		89.86		0.4
114	91.78	91.63	5.0	0.4
243		91.88		0.7
352	93.96	94.05	3.5 broad	0.3
451		94.11		0.2

Table V-11 (continued)

hkl	2θ (deg)		Line Intensity	
	Observed[a]	Calculated[b]	Observed[a]	Calculated[c]
062		95.32		0.2
541	95.51	95.56	4.5 broad	0.2
124		95.69		0.4
532	96.81	96.63	1.5 broad	0.1
162		96.84		0.2
053	98.26	98.01	4.0	0.3
361		98.42		0.6
630		99.24		0.4
343	99.36	99.47	2.5 broad	0.1
153		99.54		0.1
433 α_1	100.51	100.49	3.5	0.4
304 α_1		102.34		0.1
612 α_1	102.36	102.40	4.0	0.3
134 α_1		102.41		0.3
314 α_1	103.91	103.72	4.0	0.3
171 α_1		103.87		0.3
270 α_1	104.95	104.93	3.5	0.3
460 α_1	105.50	105.52	2.0	0.3
542 α_1	106.09	106.15	1.8	0.2
542 α_2	106.59	106.53	1.3	0.1
551 α_1	107.84	107.86	4.0	0.3
324 α_1		107.92		0.2

Table V-11 (continued)

hkl	2θ (deg) Observed[a]	2θ (deg) Calculated[b]	Line Intensity Observed[a]	Line Intensity Calculated[c]
551 α_2	108.29	108.25	2.0	0.1
324 α_2		108.31		0.1
362 α_1	109.09	109.12	1.0 broad	0.1
701 α_1	110.54	110.49	2.0	0.2
711 α_1	112.29	111.94	3.0 broad	0.1
144 α_1		112.30		0.3
632 α_1	113.79	113.76	2.0	0.3
533 α_1	115.04	114.76	3.5	0.1
172 α_1		115.02		0.1
334 α_1		115.17		0.4
721 α_1	116.39	116.37	3.0	0.4
371 α_1	116.78	116.76	2.3	0.2
721 α_2		116.83		0.2
263 α_1	120.13	120.09	5.5	0.5
272 α_1		120.12		0.3
080 α_1		120.34		0.1
462 α_1	120.72	120.78	3.0	0.3
650 α_1	122.27	122.34	1.8	0.3
712 α_1	123.92	123.83	5.0	0.3
453 α_1		123.94		0.5
712 α_2	124.52	124.37	3.0	0.1
561 α_1		124.43		0.1
453 α_2		124.48		0.3

Table V-11 (continued)

hkl	2θ (deg) Observed[a]	2θ (deg) Calculated[b]	Line Intensity Observed[a]	Line Intensity Calculated[c]
344 α_1	126.22	126.15	5.8	0.2
623 α_1		126.20		0.4
154 α_1		126.24		0.3
181 α_1		126.34		0.2
344 α_2	126.82	126.72	3.0	0.1
623 α_2		126.76		0.2
154 α_2		126.80		0.1
181 α_2		126.90		0.1
205 α_1	129.31	129.17	4.5	0.4
372 α_1		129.30		0.1
471 α_1		129.37		0.1
504 α_1		129.39		0.3
205 α_2	129.96	129.77	2.0	0.2
372 α_2		129.90		0.1
471 α_2		129.98		0.04
504 α_2		129.99		0.1
281 α_1	132.11	132.18	0.8	0.1
281 α_2	133.01	132.82	0.8	0.1
800 α_1		133.13		0.1
073 α_1	134.65	134.58	1.8	0.3
810 α_1	135.05	135.00	1.3	0.04
633 α_1		135.09		0.03
073 α_2		135.26		0.1

Table V-11 (continued)

hkl	2θ (deg) Observed[a]	2θ (deg) Calculated[b]	Line Intensity Observed[a]	Line Intensity Calculated[c]
225 α_1	136.60	136.53	6.0 broad	0.7
741 α_1		136.58		0.6
173 α_1		136.74		0.1
524 α_1		136.77		0.6
225 α_2	137.45	137.25	4.0	0.3
741 α_2		137.30		0.3
173 α_2		137.46		0.04
524 α_2		137.49		0.3
035 α_1		137.57		0.4
732 α_1	138.40	138.15	3.5 broad	0.3
035 α_2		138.31		0.2
562 α_1		138.46		0.3
082 α_1		138.54		0.2
182 α_1	141.00	140.87	4.5 broad	0.3
820 α_1		141.05		0.4
652 α_1		141.19		0.5
182 α_2	141.94	141.67	1.8 broad	0.1
820 α_2		141.86		0.2
652 α_2		142.00		0.2
354 α_1	143.44	143.28	4.5 broad	0.5
381 α_1		143.41		0.5
354 α_2	144.24	144.15	2.5 broad	0.3
381 α_2		144.28		0.2

Table V-11 (continued)

hkl	2θ (deg) Observed[a]	2θ (deg) Calculated[b]	Line Intensity Observed[a]	Line Intensity Calculated[c]
164 α_1	148.19	148.20	3.3 broad	0.6
571 α_1	150.73	150.59	6.0 broad	0.8
643 α_1		150.79		0.8
571 α_2	151.83	151.69	4.0 broad	0.4
643 α_2		151.90		0.4
480 α_1	157.97	157.83	4.0 broad	0.6
802 α_1		158.10		0.4
723 α_1	159.47	158.84	3.0 broad	0.3
480 α_2		159.33		0.3
802 α_2		159.62		0.2
751 α_1		159.72		0.3
373 α_1		159.83		0.1

[a] Two independent observers' averaged readings (2θ values are ± 0.10°) and averaged intensities on a scale from 10 to 0.

[b] Based on the orthorhombic lattice parameters a_o = 6.7162 A, b_o = 7.1031 A, c_o = 4.4084 A, and $\lambda(\bar{\alpha})$ = 1.54178 A, $\lambda(\alpha_1)$ = 1.54051 A, and $\lambda(\alpha_2)$ = 1.54433 A.

[c] Calculated using the POWD intensity program,[53] assuming the atomic coordinates of YF_3[71] for those of BkF_3, and scaled such that the most intense line had I = 10.0.

Table V-12. Line list and indexing for LaF_3-type trigonal BkF_3 (JP-VII, Film 2691A).

hkl	2θ (deg)		Line Intensity	
	Observed[a]	Calculated[b]	Observed[a]	Calculated[c]
002	24.84	24.88	8.0	3.5
110	25.44	25.49	7.0	2.5
111	28.44	28.42	10.0	10.0
112	35.84	35.92	5.5	1.3
300	44.92	44.92	9.0	3.4
113	46.02	46.06	9.0	4.3
004	51.12	51.05	4.0	0.5
302	52.02	52.03	8.0	3.1
220		52.35		0.3
221	54.02	54.01	7.5	1.9
114	57.82	57.90	4.0	0.5
222	58.72	58.80	4.0	0.4
223	66.22	66.30	7.0	1.3
304	70.30	70.32	6.0	1.2
115	71.20	71.18	6.0	0.8
410		71.41		0.3
411	72.80	72.80	7.0	1.6
224	76.20	76.14	3.0	0.2
412	76.80	76.94	3.0	0.4
006	80.50	80.53	1.5	0.2
330	82.80	82.86	3.0	0.5
413	83.70	83.68	6.5	1.4
116	86.20	86.14	4.0 broad	0.2

Table V-12 (continued)

hkl	2θ (deg) Observed[a]	2θ (deg) Calculated[b]	Line Intensity Observed[a]	Line Intensity Calculated[c]
332	88.20	88.20	7.0	0.8
225		88.24		0.5
414 α_1	92.90	92.91	4.0	0.2
306 α_1	97.18	97.21	5.0	0.5
600 α_1	99.58	99.54	3.5	0.2
117 α_1	103.48	103.44	3.0	0.3
334 α_1	104.18	104.18	3.0	0.4
602 α_1	104.98	104.98	6.0	0.4
415 α_1		105.02		0.6
602 α_2	105.38	105.35	4.0	0.2
415 α_2		105.39		0.3
521 α_1	106.58	106.62	5.0	0.6
521 α_2	107.08	107.00	3.0	0.3
522 α_1	110.78	110.83	2.0	0.2
523 α_1	118.08	118.12	6.0	0.7
523 α_2	118.58	118.60	4.0	0.3
416 α_1	120.98	120.93	1.5	0.3
227 α_1	121.56	121.59	3.0	0.3
604 α_1	122.36	122.44	3.0	0.5
441 α_1	125.16	125.27	4.0	0.4
118 α_1		125.44		0.1
441 α_2	125.96	125.83	2.0	0.2
118 α_2		126.00		0.1

Table V-12 (continued)

hkl	2θ (deg)		Line Intensity	
	Observed[a]	Calculated[b]	Observed[a]	Calculated[c]
524 α_1	129.36	129.31	3.5	0.2
524 α_2	130.06	129.92	1.5	0.1
336 α_1	135.06	135.10	4.0	0.6
443 α_1	139.76	139.71	3.5	0.5
308 α_1	140.66	140.73	5.0	0.6
308 α_2	141.66	141.53	3.0	0.3
417 α_1	144.56	144.61	6.0	1.1
417 α_2	145.56	145.51	4.0	0.5
525 α_1	147.26	147.36	6.0	1.2
525 α_2	148.36	148.34	4.0	0.6
711 α_1	150.24	150.33	6.0	1.3
711 α_2	151.44	151.43	4.0	0.6
444 α_1	157.74	157.67	2.5	0.3
712 α_1	159.84	159.79	3.0	0.6
712 α_2	161.44	161.45	1.5	0.3

[a] A single reading of the powder pattern (2θ readings are ± 0.10°). Observed intensities are on a scale of 10 to 0 and may be in error due to the presence of a second phase (orthorhombic BkF_3).

[b] Based on the trigonal lattice parameters a_o = 6.9899 A, c_o = 7.1566 A and $\lambda(\bar{\alpha})$ = 1.54178 A, $\lambda(\alpha_1)$ = 1.54051 A, and $\lambda(\alpha_2)$ = 1.54433 A.

[c] Calculated using the POWD intensity program,[53] assuming the atomic coordinates of LaF_3[70] for those of BkF_3, and scaled such that the most intense line had I = 10.0.

All of the BkF_3 powder patterns showed the presence of more than one phase. Usually all the lines were accounted for by a trigonal trifluoride phase plus an orthorhombic trifluoride phase, but in some cases other, unaccounted-for lines were present in the powder patterns. One phase was always dominant, however, and only the more intense lines of the other phases were observed. Because of the possible superposition of lines belonging to different trifluoride phases, the observed line intensities for each separate phase are subject to error. In one case (JP-VII, Film 2691A) enough of the minor YF_3-type orthorhombic phase was observed to determine lattice parameters for it.

Thoma and Brunton[75] studied the equilibrium dimorphism of the lanthanide trifluorides. Dimorphism was not observed for the trifluorides of La through Nd. They determined equilibrium inversion temperatures for the trifluorides of Sm through Lu and found them to range from 555°C for SmF_3 to 1075°C for ErF_3. The orthorhombic BkF_3 samples in this work were easily converted to the trigonal form by annealing at 600°C. The inversion temperature of BkF_3 lies between 350 and 600°C but could not be determined more precisely, since long-term annealings of trigonal BkF_3 samples failed to produce significant transformations to the orthorhombic form.

A summary of the pertinent crystallographic data of the lanthanide and actinide trifluorides, along with calculated M-F bond distances and ionic radii, is presented in Table V-13. Crystallographic data for the high-temperature form of the heavier lanthanide trifluorides is given in Ref. 75. The trifluorides of Bk and Cf are the first of the actinide trifluorides to be prepared in the YF_3-type orthorhombic modification.

By comparing the Bk^{3+} ionic radius, as calculated from the LaF_3-type trifluoride, to the similarly calculated ionic radii of the light lanthanides, it is seen that the Bk^{3+} radius fits in after Pm, the last lanthanide to exhibit the trigonal trifluoride structure below ~550°C. Alternatively, by comparing the Bk^{3+} ionic radius, as calculated from the YF_3-type trifluoride, to the similarly calculated ionic radii of the heavier lanthanides, it is seen that the Bk^{3+} radius fits in before Sm, the first lanthanide to exhibit the YF_3-type orthorhombic trifluoride structure. These calculations and comparisons assure the validity of

Table V-13. Lattice parameters, metal-fluoride bond distances, and ionic radii derived from the lanthanide and actinide trifluorides.

Trifluoride	Type	Lattice Parameters (A) a_o	b_o	c_o	Ref.	M-F Bond Distances (A) M-F(1)	M-F(2)	M-F(3)	M^{3+} Ionic Radius[a] (A) (CN = 6)
La	LaF_3	7.186		7.352	76	2.457	2.415	2.444	1.006
Ce	LaF_3	7.112		7.279	74	2.433	2.390	2.419	0.982
Pr	LaF_3	7.075		7.238	77	2.419	2.377	2.406	0.968
Nd	LaF_3	7.030		7.200	76	2.407	2.362	2.391	0.955
Pm	LaF_3	6.970		7.188	72	2.402	2.343	2.370	0.945
Sm	YF_3	6.669	7.059	4.405	71	2.622	2.328		0.921
Eu	YF_3	6.622	7.019	4.396	71	2.614	2.316		0.909
Gd	YF_3	6.570	6.984	4.393	71	2.609	2.306		0.900
Tb	YF_3	6.513	6.949	4.384	71	2.601	2.294		0.888
Dy	YF_3	6.460	6.906	4.376	71	2.594	2.282		0.877
Ho	YF_3	6.404	6.875	4.379	71	2.592	2.272		0.868
Er	YF_3	6.354	6.846	4.380	71	2.589	2.264		0.860
Tm	YF_3	6.283	6.811	4.408	71	2.599	2.257		0.855
Yb	YF_3	6.216	6.786	4.434	71	2.607	2.251		0.851
Lu	YF_3	6.151	6.758	4.467	71	2.620	2.247		0.848

Table V-13 (continued)

Trifluoride	Type	Lattice Parameters (A) a_o	b_o	c_o	Ref.	M-F Bond Distances (A) M-F(1)	M-F(2)	M-F(3)	M^{3+} Ionic Radius[a] (A) (CN = 6)
Ac	LaF_3	7.41		7.55	56	2.524	2.489	2.520	1.076
U	LaF_3	7.181		7.348	56	2.456	2.413	2.442	1.005
Np	LaF_3	7.129		7.288	56	2.436	2.395	2.425	0.986
Pu	LaF_3	7.093		7.254	56	2.425	2.383	2.412	0.974
Am	LaF_3	7.044		7.225	78	2.415	2.367	2.396	0.962
Cm	LaF_3	6.999		7.179	78	2.399	2.352	2.380	0.946
Bk	LaF_3	6.97		7.14	This	2.387	2.342	2.370	0.935
Bk	YF_3	6.70	7.09	4.41	Work	2.626	2.336		0.928
Cf	YF_3	6.653	7.041	4.395	73	2.616	2.322		0.915

[a]Calculated according to the following formula:

Ionic Radius = (weight-averaged M-F bond distance) - 1.33 - 0.11

where the fluoride ionic radius is taken to be 1.33 A[56] and the 9-fold to 6-fold coordination correction number is taken to be 0.11 A.[56]

the observed dimorphism in the BkF_3 system. It is important to note that comparisons of ionic radii can only be made meaningful if the values compared are calculated in like fashion from the same type of compound, both with respect to composition and crystal structure.

From the data in Table V-13 and by analogy with the work of Thoma and Brunton,[75] one can predict that CfF_3 will exhibit the LaF_3-type trigonal structure at temperatures greater than or equal to about 700 °C.

The calculated density (x-ray) of YF_3-type orthorhombic BkF_3 is 9.70 g/cc, whereas for the LaF_3-type trigonal modification, it is 10.15 g/cc. These numbers reflect the general trend noted in the lanthanide trifluorides that the high-temperature, trigonal modification is the more dense one.

VI. SUMMARY

The recent availability of microgram quantities of berkelium led to the beginning of a systematic study of its physical and chemical properties. Approximately 30 μg Bk^{249} were made available for this study. Since Bk^{249} decays to Cf^{249} at the rate of ~0.2% per day, repeated purification of the berkelium solution was necessary to maintain high purity. The Bk was purified by extraction from an aqueous nitrate solution with di-(2-ethylhexyl)orthophosphoric acid (HDEHP), followed by stripping of the organic phase with a hydrogen peroxide-nitric acid solution. The aqueous berkelium solution was then further purified by standard ion-exchange techniques. Purity evaluation of the resulting Bk solutions was made following each purification cycle through mass analyses, alpha pulse height analyses, Cf^{249} alpha-growth analyses, and emission spectrographic analyses. In most cases the Bk was purified to the extent that the major contaminant was from the decay of Bk^{249} itself. All experimental results were interpreted in view of the known contaminants in the Bk samples.

Absorption spectrum data were recorded over the wavelength range 300 to 2000 mμ for Bk^{3+} absorbed in single beads of cation-exchange resin. Lack of resolution in the bead spectra led to the development of a "suspended-drop", microabsorption cell, where ~4 μg Bk^{249} in a few nanoliters of dilute HCl solution were suspended between two small, quartz rods. Once loaded, the cell was placed in the Cary Spectrophotometer, and spectra were taken over the wavelength range 300 to 700 mμ in all cases, and in some cases, over the range 260 to 1200 mμ. The composite results of these spectra yielded 16 peaks between 320 and 700 mμ. The two most intense peaks observed were at 418 and 474 mμ. Limited resolution in the Bk^{3+} solution absorption spectrum, coupled with the complexity of the theoretically derived Bk^{3+} absorption spectrum in the ultraviolet region, prevented the assignment of J-values to the various electronic energy levels experimentally determined.

An attempt to observe the Bk^{4+} solution absorption spectrum, by electrolytically oxidizing the Bk^{3+} in HNO_3 solution, was unsuccessful. The failure was attributed to the rapid reduction of the Bk^{4+} ions, formed locally at the anode, by radiolytically generated H_2O_2 in the bulk of the solution.

Freshly purified Bk was loaded to saturation (~0.2 μg) in single beads of ion-exchange resin for air-calcination to BkO_2 at a temperature of ~1200°C. Dry hydrogen gas reduction of these dioxide samples at 600°C produced the cubic Bk_2O_3. Anhydrous $BkCl_3$ samples were prepared from the sesquioxides by treatment with HCl gas at 520°C. Conversion to BkOCl was carried out by treatment of the trichlorides in an appropriate $HCl_{(g)}$-$H_2O_{(g)}$ mixture at 500°C. BkF_3 samples were prepared by treatment of the berkelium oxides with a $H_{2(g)}$-$HF_{(g)}$ mixture at 600°C. Low-temperature BkO_2 samples were readily prepared by heating any of the berkelium oxides, halides, or oxyhalides in air or oxygen at 600°C.

All compound samples prepared were examined by standard x-ray powder techniques. In all cases BkO_2 exhibited the fluorite-type, face-centered cubic structure with the "purest" sample yielding a lattice parameter $a_o = 5.334 \pm 0.001$ A. The dioxide stoichiometry was assumed, as was that of the Mn_2O_3-type cubic sesquioxide. The "purest" sample of Bk_2O_3 yielded a cubic lattice parameter $a_o = 10.889 \pm 0.003$ A. These lattice parameter error limits represent the 95% confidence interval reflecting only the internal consistency of the data for these particular preparations. The effect of time on the berkelium oxide lattice parameters was studied. The lattice parameter of BkO_2 increased with time, while that of Bk_2O_3 decreased.

$BkCl_3$ exhibited the UCl_3-type hexagonal structure. The lattice parameters of $BkCl_3$ are $a_o = 7.382 \pm 0.002$ A and $c_o = 4.127 \pm 0.003$ A. Samples of BkOCl exhibited the PbFCl-type tetragonal structure. The lattice parameters of BkOCl are $a_o = 3.966 \pm 0.004$ A and $c_o = 6.710 \pm 0.009$ A. The lattice parameter error limits reported for $BkCl_3$ and BkOCl are the 95% confidence interval calculated using the standard statistical method for the average of three independent determinations.

BkF_3 samples exhibited two crystal structures, a low-temperature, YF_3-type orthorhombic structure and a high-temperature, LaF_3-type trigonal structure. "Best estimates" for the lattice parameters of these two BkF_3 modifications are: $a_o = 6.70 \pm 0.01$ A, $b_o = 7.09 \pm 0.01$ A, $c_o = 4.41 \pm 0.01$ A (orthorhombic), and $a_o = 6.97 \pm 0.01$ A, $c_o = 7.14 \pm 0.01$ A (trigonal).

The lattice parameter error limits reported here are empirical, reflecting the uncertainties in the derivation of the lattice parameters.

Comparisons of the lattice parameters of these berkelium compounds with those of isostructural actinide compounds consistently showed evidence of the "actinide contraction". Values of the Bk^{3+} radius were calculated from the crystallographic data of the berkelium halides and sesquioxide. The variability of these Bk^{3+} radius values reflects the limitations of the ionic radius concept.

ACKNOWLEDGMENTS

Very special notes of thanks go to Dr. Jere L. Green and Professor Burris B. Cunningham. Dr. Green introduced me to the fascinating world of submicrogram techniques and patiently taught me the "tricks of the trade". Professor Cunningham was a constant source of help throughout this study. His many helpful suggestions, his encouragement and personal interest, his developmental work on the light-pipe, microabsorption cell, and his assistance during the spectroscopic studies are all gratefully acknowledged. Under Professor Cunningham's guidance my postgraduate studies became a most enjoyable, educational experience.

Dr. Sherman Fried is thanked for his capillary salt-bridge cathode system, used during the Bk^{4+} spectroscopic work, and for his other helpful suggestions. The suggestions and assistance of Mr. Tom C. Parsons, especially during the spectroscopic studies, were most helpful. The analytical work of Dr. Maynard C. Michel (mass analyses) and Mr. George Shalimoff (mass analyses and emission spectrographic analyses) was greatly appreciated and was crucial to the completion of this work.

Miss Judy C. Copeland is thanked for her assistance during the compound preparation and film-reading phases of this work. I would also like to thank Mr. Dennis K. Fujita and Mr. David Temple for their film-reading help.

In addition, thanks to Mr. Tommy R. Corbin, for his efforts in developing the radiation detection equipment, to Mr. Will D. Phillips, for his design of the glove-box modifications and safety equipment, and to Mrs. Gertrude R. Bolz, for her careful monitoring assistance and concern for safety.

Miss Lilly Y. Goda and Mrs. Lillian B. White are sincerely thanked for their laboratory assistance during all phases of this work.

Final notes of thanks go to the other members of the lanthanide and actinide chemistry group, who often contributed helpful suggestions or constructive criticisms, and to my family and friends, whose moral support and continuous encouragement made my work easier.

This work was done under the auspices of the U. S. Atomic Energy Commission.

REFERENCES

1. E. K. Hulet, J. Inorg. Nucl. Chem. 26, 1721 (1964).
2. J. Kooi, R. Boden, and J. Wijkstra, J. Inorg. Nucl. Chem. 26, 2300 (1964).
3. S. G. Thompson, B. B. Cunningham, and G. T. Seaborg, J. Am. Chem. Soc. 72, 2798 (1950).
4. S. G. Thompson, A. Ghiorso, and G. T. Seaborg, Phys. Rev. 80, 781 (1950).
5. C. Musikas and R. Berger, presented to the American Chemical Society meeting, New York (September 1966).
6. M. E. Jones and B. B. Cunningham, University of California Lawrence Radiation Laboratory Report, AECD-2913 (1950).
7. J. Milsted, A. M. Friedman, and C. M. Stevens, Nucl. Phys. 71, 299 (1965).
8. S. E. Vandenbosch, H. Diamond, R. K. Sjoblom, and P. R. Fields, Phys. Rev. 115, 115 (1959).
9. T. A. Eastwood, J. P. Butler, M. J. Cabell, H. G. Jackson, R. P. Schuman, F. M. Rourke, and T. L. Collins, Phys. Rev. 107, 1635 (1957).
10. L. B. Magnuson, M. H. Studier, P. R. Fields, C. M. Stevens, J. F. Mech, A. M. Friedman, H. Diamond, and J. R. Huizenga, Phys. Rev. 96, 1576 (1954).
11. A. Chetham-Strode and R. J. Silva, Oak Ridge National Laboratory Report, ORNL-3679 (1964).
12. E. K. Hulet, S. G. Thompson, and A. Ghiorso, Phys. Rev. 95, 1703 (1954).
13. E. K. Hulet, S. G. Thompson, A. Ghiorso, and K. Street, Jr., Phys. Rev. 84, 366 (1951).
14. A. Chetham-Strode, Jr., (Ph.D. Thesis), University of California Lawrence Radiation Laboratory Report, UCRL-3322 (1956).
15. E. K. Hyde and G. T. Seaborg, University of California Lawrence Radiation Laboratory Report, UCRL-3312 (1956).
16. C. M. Lederer, J. M. Hollander, and I. Perlman, Table of Isotopes, 6th Edition, John Wiley and Sons, Inc., New York (1967).
17. B. B. Cunningham, J. Chem. Ed. 36, 32 (1959).
18. B. B. Cunningham, Proc. of the Robert A. Welch Foundation Conference on Chemical Research, VI, Topics in Modern Inorganic Chemistry (1962).

19. R. G. Gutmacher, E. K. Hulet, and R. Lougheed, J. Opt. Soc. Am. 55, 1029 (1965).
20. R. G. Gutmacher, E. K. Hulet, R. Lougheed, J. G. Conway, W. T. Carnall, D. Cohen, T. K. Keenan, and R. D. Baybarz, J. Inorg. Nucl. Chem. 29, 2341 (1967).
21. B. B. Cunningham, Microchemical Journal, Symposium (1961).
22. S. G. Thompson, A. Ghiorso, and G. T. Seaborg, Phys. Rev. 77, 838 (1950).
23. G. T. Seaborg and A. R. Fritsch, "The Synthetic Elements: III", Scientific American, W. H. Freeman and Co., San Francisco (April 1963).
24. F. L. Moore, Anal. Chem. 37, 1235 (1965).
25. G. H. Higgins, University of California Lawrence Radiation Laboratory Report, UCRL-6134 (1960).
26. D. F. Peppard, S. W. Moline, and G. W. Mason, J. Inorg. Nucl. Chem. 4, 344 (1957).
27. E. K. Hulet, J. Inorg. Nucl. Chem. 26, 1721 (1964).
28. D. B. McWhan, B. B. Cunningham, and J. C. Wallmann, J. Inorg. Nucl. Chem. 24, 1025 (1962).
29. J. L. Green, (Ph.D. Thesis), University of California Lawrence Radiation Laboratory Report, UCRL-16516 (November 1965).
30. J. T. Haley, R. J. Walker, and T. R. Corbin, University of California Lawrence Radiation Laboratory Report, UCRL-16869 (1966).
31. R. J. Walker and T. R. Corbin, University of California Lawrence Radiation Laboratory Report, UCRL-16467 (1965).
32. S. G. Thompson, B. G. Harvey, G. R. Choppin, and G. T. Seaborg, J. Am. Chem. Soc. 76, 6229 (1954).
33. H. L. Smith and D. C. Hoffman, J. Inorg. Nucl. Chem. 3, 243 (1956).
34. J. P. Surls, Jr., University of California Lawrence Radiation Laboratory Report, UCRL-3209 (1956).
35. R. M. Diamond, K. Street, Jr., and G. T. Seaborg, J. Am. Chem. Soc. 76, 1461 (1954).
36. Referenced in 29. to J. Milsted, Argonne National Laboratory, private communication (1965).
37. M. G. Inghram, Ann. Rev. Nucl. Sci. 4, 81 (1954).
38. Irshad Ahmad, (Ph.D. Thesis), University of California Lawrence Radiation Laboratory Report, UCRL-16888 (September 1966).

39. R. J. Barrett, "Table of Specific Activities of Selected Isotopes", based on the General Electric Chart of the Nuclides, revised to June 1964 (1965).

40. R. G. Gutmacher, E. K. Hulet, E. F. Worden, and J. G. Conway, J. Opt. Soc. Am. 53, 506 (1963).

41. R. G. Gutmacher, University of California Lawrence Radiation Laboratory Report, UCRL-12275-T (1964).

42. J. L. Green and B. B. Cunningham, Inorg, Nucl. Chem. Letters 2, 365 (1966).

43. D. C. Stewart, University of California Lawrence Radiation Laboratory Report, AECD-2389 (1948).

44. B. B. Cunningham, J. R. Peterson, R. D. Baybarz, and T. C. Parsons, University of California Lawrence Radiation Laboratory Report, UCRL-17692 (1967) (submitted to Inorg. Nucl. Chem. Letters).

45. P. R. Fields, B. G. Wybourne, and W. T. Carnall, Argonne National Laboratory Report, ANL-6911 (1964).

46. W. T. Carnall and B. G. Wybourne, J. Chem. Phys. 40, 3428 (1964).

47. J. G. Conway, University of California Lawrence Radiation Laboratory, unpublished results (1966).

48. B. G. Wybourne, Spectroscopic Properties of Rare Earths, Interscience Publishers, New York (1965).

49. C. W. Koch, (Ph.D. Thesis), University of California Lawrence Radiation Laboratory Report, UCRL-2286 (September 1953).

50. W. Parrish and E. Cisney, Philips Tech. Rev. 10, 157 (1948).

51. J. D. H. Donnay, Editor, Crystal Data, 2nd Edition, American Crystallographic Association, ACA Monograph No. 5 (1963).

52. R. W. G. Wyckoff, Crystal Structures, Volume I, Chapter II, Interscience Publishers, Inc., New York (1960).

53. D. K. Smith, University of California Lawrence Radiation Laboratory Report, UCRL-7196 (1963).

54. A. C. Larson, R. B. Roof, Jr., and D. T. Cromer, Los Alamos Scientific Laboratory Report, LA-3335 (1965).

55. D. E. Williams, Ames Laboratory Report, IS-1052 (1964).

56. W. H. Zachariasen, The Actinide Elements, Chap. 18, National Nuclear Energy Series, Vol. IV-14A, McGraw-Hill Book Co., Inc., New York (1954).

57. L. Pauling and M. D. Shappell, Z. Krist. 75, 128 (1930).
58. J. C. Copeland, (M.S. Thesis), University of California Lawrence Radiation Laboratory Report, UCRL-17718 (August 1967).
59. D. H. Templeton and C. H. Dauben, J. Am. Chem. Soc. 76, 5237 (1954).
60. A. F. Wells, Structural Inorganic Chemistry, Chap. XXVII, Oxford University Press, London (1962).
61. J. L. Green and B. B. Cunningham, Inorg. Nucl. Chem. Letters 3, 343 (1967).
62. W. H. Zachariasen, The Transuranium Elements, Part II, National Nuclear Energy Series, Vol. 14B, Paper 20.6, McGraw-Hill Book Co., Inc., New York (1949).
63. W. H. Zachariasen, Acta. Cryst. 1, 265 (1948).
64. J. D. Forrester, Allan Zalkin, D. H. Templeton, and J. C. Wallmann, Inorg. Chem. 3, 185 (1964).
65. D. H. Templeton and G. F. Carter, J. Phys. Chem. 58, 940 (1954).
66. W. Nieuwenkamp and J. M. Bijvoet, Z. Krist. 81, 469 (1931).
67. D. H. Templeton and C. H. Dauben, J. Am. Chem. Soc. 75, 6069 (1953).
68. D. H. Templeton and C. H. Dauben, J. Am. Chem. Soc. 75, 4560 (1953).
69. S. A. Shchukarev and A. I. Efimov, Zhur. Neorg. Khim. 2, 2304 (1957).
70. Allan Zalkin, David H. Templeton, and Ted. E. Hopkins, Inorg. Chem. 5, 1466 (1966).
71. Allan Zalkin and D. H. Templeton, J. Am. Chem. Soc. 75, 2453 (1953).
72. Fritz Weigel, "Präparative und röntgenographische Untersuchungen an stark radioaktiven Stoffen", University of Munich, Munich (1965).
73. J. R. Peterson, J. C. Copeland, and D. Temple, University of California Lawrence Radiation Laboratory, unpublished results (1967).
74. H. E. Swanson et al., National Bureau of Standards Circular No. 539, Vol. 8, U. S. Government Printing Office, Washington, D. C. (1959); ASTM X-ray Diffraction Card No. 8-45.
75. R. E. Thoma and G. D. Brunton, Inorg. Chem. 5, 1937 (1966).
76. E. Staritzky and L. B. Asprey, Anal. Chem. 29, 856 (1957).
77. H. E. Swanson et al., National Bureau of Standards, ASTM X-ray Diffraction Card No. 6-0325.
78. L. B. Asprey, T. K. Keenan, and F. H. Kruse, Inorg. Chem. 4, 985 (1965).